



**HAL**  
open science

## Modelling the adsorption of phenolic acids onto $\alpha,\gamma$ -alumina particles

Pauline Moreau, Sonia Collette-Maatouk, Pierre Gareil, Pascal E. Reiller

► **To cite this version:**

Pauline Moreau, Sonia Collette-Maatouk, Pierre Gareil, Pascal E. Reiller. Modelling the adsorption of phenolic acids onto  $\alpha,\gamma$ -alumina particles. *Colloids and Surfaces A: Physicochemical and Engineering Aspects*, 2013, 435, pp.97-108. 10.1016/j.colsurfa.2013.02.035 . cea-00852745

**HAL Id: cea-00852745**

**<https://cea.hal.science/cea-00852745>**

Submitted on 13 Sep 2019

**HAL** is a multi-disciplinary open access archive for the deposit and dissemination of scientific research documents, whether they are published or not. The documents may come from teaching and research institutions in France or abroad, or from public or private research centers.

L'archive ouverte pluridisciplinaire **HAL**, est destinée au dépôt et à la diffusion de documents scientifiques de niveau recherche, publiés ou non, émanant des établissements d'enseignement et de recherche français ou étrangers, des laboratoires publics ou privés.



Distributed under a Creative Commons Attribution - NonCommercial - ShareAlike 4.0 International License

# Modelling the adsorption of phenolic acids onto $\alpha,\gamma$ -alumina particles

---

Pauline Moreau<sup>a</sup>, Sonia Colette-Maatouk<sup>a</sup>, Pierre Gareil<sup>b</sup>, Pascal E. Reiller<sup>a,\*</sup>

<sup>a</sup> Commissariat à l'Énergie Atomique et aux énergies alternatives, CE Saclay, CEA/DEN/DANS/DPC/SEARS, Laboratoire de développement Analytique, Nucléaire, Isotopique et Élémentaire, Bâtiment 391 PC 33, F-91191 Gif-sur-Yvette CEDEX, France.

<sup>b</sup> Chimie ParisTech, Laboratory of Physicochemistry of Electrolytes, Colloids, and Analytical Sciences, CNRS UMR 7195, 75005, Paris, France.

\* corresponding author : pascal.reiller@cea.fr, tel +33 1 6908 4312

Colloids and Surfaces A: Physicochemical and Engineering Aspects 435, 97-108

<http://doi.org/10.1016/j.colsurfa.2013.02.035>

---

## ABSTRACT

Adsorption of three phenolic acids, namely parahydroxybenzoic acid (4-hydroxybenzoic acid, H<sub>2</sub>Phb), protocatechuic acid (3,4-dihydroxybenzoic acid, H<sub>2</sub>Proto) and gallic acid (3,4,5-trihydroxybenzoic acid, H<sub>2</sub>Gal) onto  $\alpha,\gamma$ -Al<sub>2</sub>O<sub>3</sub> particles was studied *vs.* ligand concentration at pH 5.0, and *vs.* pH. The oxide surface was characterized with both potentiometric titrations and electrophoretic measurements; a difference in the point of zero salt effect (PZSE) and the isoelectric point (IEP) was evidenced, which could be attributed to the presence of impurities or to the heterogeneity of the oxide. The potentiometric titration experiments lead to the determination of a PZSE of 8.5. Moreover, the particular shape of the curves were fitted in the framework of the constant capacitance model (CCM), using FITEQL 4.0 software, to determine the oxide parameters (protolytic properties and site density). The electrophoretic measurements were fitted in the framework of the double diffuse layer model (DLM) and an IEP of 9.5 was determined. The constant-pH isotherms of the acids were fitted using the CCM. Constant-pH isotherms of H<sub>2</sub>Gal and H<sub>2</sub>Proto onto the Al<sub>2</sub>O<sub>3</sub> surface sites at pH 5 were similar. Two adsorption sites of different affinities were clearly evidenced for H<sub>2</sub>Gal and can also be proposed for H<sub>2</sub>Proto. H<sub>2</sub>Phb showed a lower affinity for the surface than the two other acids, as the logK<sub>sorb</sub> for H<sub>2</sub>Phb is one and a half time lower than the one for H<sub>2</sub>Proto when adsorption is described with one adsorption site. As expected for a carboxylic acid, adsorption of H<sub>2</sub>Phb decreased with pH and experimental data were well fitted using three adsorbed species ( $\equiv\text{MOH}_2\text{H}_2\text{Phb}^+$ ,  $\equiv\text{MHPb}^-$ , and  $\equiv\text{MPhb}^-$ ). Adsorption of H<sub>2</sub>Proto and H<sub>2</sub>Gal did not change significantly upon increasing pH, meaning that the different functional groups on the aromatic ring (carboxylate and phenolate) were involved in adsorption as pH increases. Dissolution of the oxide was also estimated by measuring the amount of soluble aluminum at pH 5. Increasing acid concentration promoted dissolution, especially for the low concentration range ([acid] < 3 mmol.L<sup>-1</sup>), but higher acid concentration lowers the increase of the solubility increase, likely

due to adsorption on surface of an aluminum-organic complex.

## 1 INTRODUCTION

Understanding adsorption processes of organic molecules, containing both carboxylate and phenolate moieties, onto oxide colloids is relevant for environmental issues. Indeed, these chemical functions are abundant in nature, as for example in decomposition products of lignin, among them phenolic acids, and afterwards in humic and fulvic acids. Such molecules are involved in several geochemical processes, such as complexation with metal-ions [1-8], oxide dissolution [9-13] and pH buffering. Among phenolic acids of relevance are parahydroxybenzoic acid (4-hydroxybenzoic acid, H<sub>2</sub>Phb), protocatechuic acid (3,4-dihydroxybenzoic acid, H<sub>2</sub>Proto) and gallic acid (3,4,5-trihydroxybenzoic acid, H<sub>2</sub>Gal): only the two lowest pK<sub>a</sub> of the acids are reflected in the acronyms and the complete formulae are given in Figure 1. Indeed, they were evidenced in several humus of soils and in fruit peels [14-20] and these three acids differ only by adding an OH group on the aromatic ring. Adsorption of organic acids onto oxides is maximum for pH values around the pK<sub>a</sub> of acids [10,21-24] and depends on several parameters such as pH, ionic strength, and number and position of ionizable polar functional groups [21,24-32].

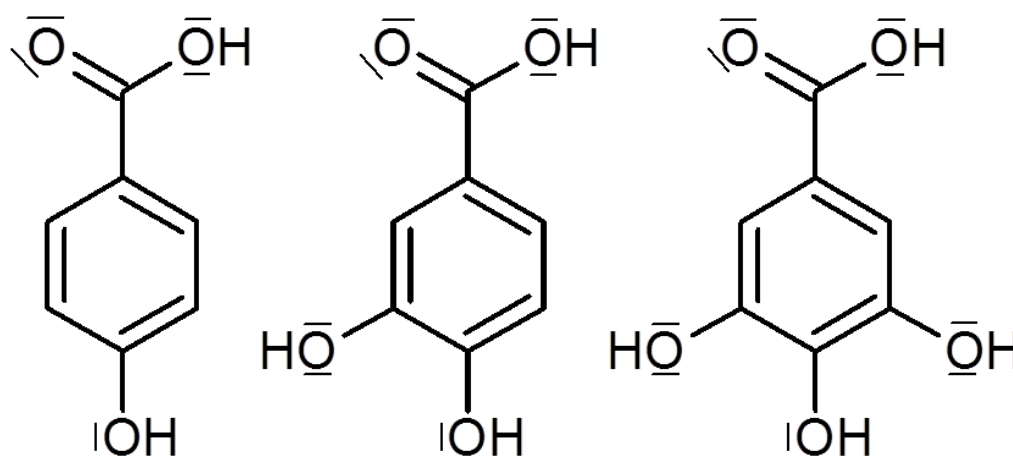


Figure 1. H<sub>2</sub>Phb, H<sub>2</sub>Proto, H<sub>2</sub>Gal (from left to right)

It has been shown that the adsorption of H<sub>2</sub>Phb onto several oxides is high for low pH and decreases with increasing pH, as for example onto Al<sub>2</sub>O<sub>3</sub> [26,30], goethite [27], and hematite [29]. Adsorption of H<sub>2</sub>Phb onto various iron oxides (non-crystalline, hematite, goethite, ferrihydrite) greatly depends upon the oxide nature, crystalline phases, density and accessibility of the sites [25]. Analysis by IR spectroscopy showed that the carboxylic function of H<sub>2</sub>Phb interacts with the surface as a bidentate surface complex, involving the two carboxylic oxygens (O<sub>carb</sub>) [29]. Conversely, the phenolic oxygen (O<sub>phen</sub>) is not deprotonated and does not interact with oxide surface [29,30]. Das *et al.* [30] proposed that the surface complex formed by adsorption of H<sub>2</sub>Phb onto Al<sub>2</sub>O<sub>3</sub> is outer-sphere in the pH range 5-6, whereas it is inner-sphere at pH 7-9.

Guan *et al.* [33] showed that adsorption of dihydroxybenzoic acids at pH 6 decreases as the pK<sub>a</sub> of the acids increases; among the five dihydroxybenzoic acids studied by these authors, H<sub>2</sub>Proto

is the least sorbed onto aluminum oxides. Attenuated total reflectance-Fourier transformed infrared spectroscopy (ATR-FTIR) analysis showed that H<sub>2</sub>Proto was sorbed onto Al<sub>2</sub>O<sub>3</sub> forming bidentate mononuclear complexes, involving the carboxylate group of H<sub>2</sub>Proto for pH < 7 and the two phenolate groups as pH increases [31,33]. For H<sub>2</sub>Gal, Evanko and Dzombak [27] showed that adsorption onto goethite is approximately constant as a function of pH. However, to our knowledge, no constant-pH isotherm of this latter acid has been described yet. Adsorption of salicylic acid (2-hydroxybenzoic acid) onto oxides [21,26,28,34,35] is greater than that of H<sub>2</sub>Phb [26,28,30], due to the chelate formation [26]. It cannot give direct information on the influence of distal phenolic groups.

Pure Al<sub>2</sub>O<sub>3</sub> does not often occur in nature but its surface sites have similar properties as aluminol sites in non-stratified clays [36] and as iron oxide with respect to metal ion adsorption [37,38]. Moreover, a large body of organic acid adsorption works exists, which can be used for comparison [10,21-24,26-28,30,31,33-35]. Hence, our aim was to probe the role of the number of phenolate group for adsorption of phenolic acids (H<sub>2</sub>Phb, H<sub>2</sub>Proto and H<sub>2</sub>Gal, hereafter noted H<sub>2</sub>A, i.e., only the two proton will be apparent) onto aluminum oxide. We will use the simplest electrostatic models to describe the electrochemistry of our surface in a semi-operational objective, i.e. to obtain the lowest set of sound parameters that permits to describe our system: the constant capacitance model (CCM) and the double diffuse layer model (DLM). Samples containing mineral surface and one phenolic acid will be hereafter called 'binary systems'.

## 2 EXPERIMENTAL SECTION

### 2.1 PREPARATION OF SAMPLES

All solutions were prepared using freshly purified water (18.2 MΩ.cm) delivered by a Thermo EASYPURE II apparatus (Saint Herblain, France). H<sub>2</sub>Phb, H<sub>2</sub>Proto, H<sub>2</sub>Gal and NaCl were purchased from Sigma-Aldrich (Saint-Quentin-Fallavier, France) and were used as received. Stock solutions of the phenolic acids (10<sup>-2</sup> mol.L<sup>-1</sup> for H<sub>2</sub>Phb and 2 10<sup>-2</sup> mol.L<sup>-1</sup> for H<sub>2</sub>Proto, and 10<sup>-2</sup> mol.L<sup>-1</sup> for H<sub>2</sub>Gal) were obtained after dissolution in 0.01 mol.L<sup>-1</sup> NaCl. The pK<sub>a</sub> of the carboxylic acid functions are 4.58, 4.49, and 4.44, for H<sub>2</sub>Phb, H<sub>2</sub>Proto, and H<sub>2</sub>Gal, respectively [16], and the pK<sub>a</sub> of the first phenolic functions are 9.46, 8.75 and 9.11, for H<sub>2</sub>Phb, H<sub>2</sub>Proto, and H<sub>2</sub>Gal, respectively [16]. The other pK<sub>a</sub>'s of protocatechuic and gallic acids were considered too high to be ionized under our experimental conditions. The pK<sub>a</sub> values are corrected of ionic strength using the Davies equation [39].

Dry Al<sub>2</sub>O<sub>3</sub> particles (predominantly γ phase, 5-20% α phase, pure 99.98% metal basis, mean particle size 0.26 μm, BET specific surface area 110 m<sup>2</sup>/g) were purchased from Alfa Aesar (Schiltigheim, France). Thermodynamic constants for aluminum phases and Al<sup>3+</sup> hydrolysis are recalled in Table 1, and are corrected at desired ionic strength using the Davies equation [39]. Solid stock suspensions were prepared in a glovebox by introducing the Al<sub>2</sub>O<sub>3</sub> powder in 30 mL of 0.01 mol.L<sup>-1</sup> NaCl, acidified by HCl to pH 4. The suspensions were then sonicated at amplitude 6 for 10 min with a Misonix sonicator 4000 (Misonix Sonicators, Newton, USA) equipped with a cup horn thermostated at 8°C. The suspensions were stirred for

at least 7 days before use to allow equilibration of the surface [44]. Sonication was repeated just before preparation of the binary systems.

Table 1. Stability constants at 25°C for different oxo-hydroxo aluminium(III) phases and solution speciation of Al(III).

Solubility constant for oxo-hydroxo aluminium(III) phases			
Oxide	Reaction	$\log_{10}K_s (I=0)$	Ref
$\alpha$ -Al <sub>2</sub> O <sub>3</sub>	$\text{Al}_2\text{O}_3 + 6 \text{H}^+ \rightleftharpoons 2 \text{Al}^{3+} + 3 \text{H}_2\text{O}$	18.33	[40]
$\gamma$ -Al <sub>2</sub> O <sub>3</sub>	$\text{Al}_2\text{O}_3 + 6 \text{H}^+ \rightleftharpoons 2 \text{Al}^{3+} + 3 \text{H}_2\text{O}$	21.49	[41]
Bayerite	$\text{Al}(\text{OH})_3 + 3\text{H}^+ \rightleftharpoons \text{Al}^{3+} + 3\text{H}_2\text{O}$	8.62	[42]
Boehmite	$\text{AlOOH} + 3 \text{H}^+ \rightleftharpoons \text{Al}^{3+} + 2 \text{H}_2\text{O}$	7.74	[42]
Solution speciation of Al(III)			
Reaction		$\log_{10}^*\beta_n^{\circ} (I=0)$	Ref
$\text{Al}^{3+} + \text{H}_2\text{O} \rightleftharpoons \text{AlOH}^{2+} + \text{H}^+$		-4.99	[43]
$\text{Al}^{3+} + 2\text{H}_2\text{O} \rightleftharpoons \text{Al}(\text{OH})_2^+ + 2\text{H}^+$		-10.20	[43]
$\text{Al}^{3+} + 3\text{H}_2\text{O} \rightleftharpoons \text{Al}(\text{OH})_3 + 3\text{H}^+$		-15.73	[43]
$\text{Al}^{3+} + 4\text{H}_2\text{O} \rightleftharpoons \text{Al}(\text{OH})_4^- + 4\text{H}^+$		-22.90	[43]

## 2.2 POTENTIOMETRIC TITRATION OF Al<sub>2</sub>O<sub>3</sub>

All potentiometric titrations of Al<sub>2</sub>O<sub>3</sub> suspensions were performed using a Titrand 809 computer-controlled system equipped with 10 mL burettes and pH meter (Metrohm, Villebon, France) under decarbonated N<sub>2</sub> atmosphere, at 20°C; the gas flow was successively bubbled through 0.1 mol.L<sup>-1</sup> NaOH, 0.1 mol.L<sup>-1</sup> HCl, and 0.01 mol.L<sup>-1</sup> NaCl. The electrodes (Metrohm, 60726107 used as a reference and 60150100 as pH indicator) were calibrated using four commercial buffer solutions (pH 1.68, 4.01, 7.01, 10.00, Fisher Scientific, Illkirch, France). The titrated suspensions (20 mL) were composed of C<sub>Al<sub>2</sub>O<sub>3</sub></sub> = 10 g.L<sup>-1</sup> in 0.01, 0.1, and 0.25 mol.L<sup>-1</sup> NaCl. The pH of the suspensions was first set to 4 and then increased to 11 by stepwise additions of 0.1 mol.L<sup>-1</sup> NaOH. Depending on the maximum electrode drift (0.1 mV/min), the maximum time intervals between additions was fixed at 300 s. The suspensions were titrated by adding 10  $\mu$ L of titrant, and pH was recorded as a function of the amount of added titrant, knowing that the volume of titrant added is the experimental factor that impacts the results the most [45]. Titrations of the electrolytes alone (blank titrations) were performed under the same experimental conditions to take into account all the acid-base properties of the electrolyte and other parameters such as the junction potential at the electrodes [46], and to determine the activity coefficients for H<sup>+</sup> ( $\gamma_{\text{H}^+}$ ) and OH<sup>-</sup> ( $\gamma_{\text{OH}^-}$ ). Then, the real quantity of exchanged protons was calculated by subtracting the blank curve to experimental data. The experimental data were then corrected so that sorbed H<sup>+</sup> concentration is nil at the intersection point (PZSE) of the titration curves performed at the three ionic strengths.

From thermodynamic data (Table 1)  $\gamma$ -Al<sub>2</sub>O<sub>3</sub> is not stable at 25°C and should undertake extensive phase change to boehmite,  $\gamma$ -AlO(OH), or to bayerite,  $\beta$ -Al(OH)<sub>3</sub> [44,47]. The

dissolution of our mineral within the time frame of our experiments seems to more be controlled by either  $\alpha$ - $\text{Al}_2\text{O}_3$  or bayerite (*vide post*) and solubilization should be minimum within the pH range 4.2-11; influence of dissolution on the total number of sites can be neglected in the pH range 5-10.

The experimental data were fitted using the FITEQL 4.0 software [48] in the framework of the constant capacitance model (CCM). The accuracy of fit was checked by the overall variance (the weighted sum of squares of residuals divided by the degree of freedom, WSOS/D). A value of less than 20 is common for an acceptable fit [48]. The capacitance value was adjusted by a trial-and-error approach in order to minimize WSOS/D. The other parameters, namely the surface ionisation constants ( $K_1$  and  $K_2$ ) and the site density ( $N_s$ ) of the oxide, were determined by adjustment for minimum WSOS/D for the three ionic strengths.

### 2.3 ELECTROPHORETIC MOBILITY MEASUREMENTS

Electrophoretic mobilities of particles were measured at different pH values using a NanoZS Zetasizer (Malvern Instruments, Orsay, France) equipped with a Malvern ZEN1010 cell permitting measurements at high concentrations without degradation of the samples. The voltage was set to 50 V both in ‘fast field reversal mode’ to determine the electrophoretic mobility, and in ‘slow field reversal mode’ to determine dispersion around the value. The optimal  $C_{\text{Al}_2\text{O}_3} = 0.5 \text{ g.L}^{-1}$  for mobility measurements was chosen. The suspensions containing 100 mL of  $C_{\text{Al}_2\text{O}_3} = 0.5 \text{ g.L}^{-1}$  with ionic strengths of 0.01 and 0.05 mol.L<sup>-1</sup> (NaCl) were titrated by adding negligible amounts of 1 mol.L<sup>-1</sup> NaOH or HCl (total added volume < 1 mL). During titration, the sample was continuously stirred.

### 2.4 PREPARATION OF PHENOLIC ACIDS/ $\text{Al}_2\text{O}_3$ BINARY SYSTEMS

Stock solutions of phenolic acids and stock suspension of  $\text{Al}_2\text{O}_3$  were used. The pH values were measured using a combined glass electrode (Mettler-Toledo, Viroflay, France) connected to a Seven Easy S20 Mettler-Toledo pH meter: the electrode was calibrated using three commercial buffer solutions (Mettler-Toledo, pH 4.01, 7.01, and 10.00). In all samples, pH was adjusted by adding drops of 1 mol.L<sup>-1</sup> HCl or NaOH. Constant-pH isotherms of acids onto  $\text{Al}_2\text{O}_3$  were obtained at pH 5.0, at a fixed ionic strength ( $I$ ) of 0.01 mol.L<sup>-1</sup> NaCl, with an  $\text{Al}_2\text{O}_3$  concentration  $C_{\text{Al}_2\text{O}_3} = 0.5 \text{ g.L}^{-1}$  for the three acids and with  $C_{\text{Al}_2\text{O}_3} = 5 \text{ g.L}^{-1}$  for  $\text{H}_2\text{Phb}$ . The so-called ‘pH-isotherms’ of the acids were obtained at  $10^{-3} \text{ mol.L}^{-1}$  for  $\text{H}_2\text{Phb}$ ,  $8 \cdot 10^{-4} \text{ mol.L}^{-1}$  for  $\text{H}_2\text{Proto}$  and  $10^{-3} \text{ mol.L}^{-1}$  for  $\text{H}_2\text{Gal}$ ,  $C_{\text{Al}_2\text{O}_3} = 0.5 \text{ g.L}^{-1}$ , and  $I = 0.01 \text{ mol.L}^{-1}$  NaCl. The binary samples were equilibrated under stirring for 3 days [30,31] before centrifugation at 10 000 rpm for 90 min. Only the top 5 cm supernatant (out of the total 6.5 cm) was collected for analysis to avoid a remixing of small particles with the supernatant after centrifugation.

## 2.5 DETERMINATION OF THE PHENOLIC ACID CONCENTRATION BY UV-VISIBLE SPECTROSCOPY

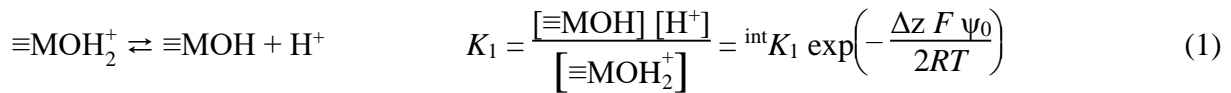
Absorbance spectra of the acids were recorded in a 1 cm quartz cuvette using a UV2550PC-CE Spectrophotometer (Shimadzu, Marne-la-Vallée, France). UV/Vis spectra were recorded at 20°C between 200 and 600 nm and pH of all studied samples was set to 5 by adding drops of 1 mol.L<sup>-1</sup> HCl or NaOH before acquisition. The acid concentrations were determined at 247, 253 and 260 nm for H<sub>2</sub>Phb, H<sub>2</sub>Proto and H<sub>2</sub>Gal, respectively. Acid concentrations in the supernatant were determined from 7-points calibration curves from 8 to 200 μmol.L<sup>-1</sup>. Some samples were diluted before analysis to meet the calibration curve concentration criterion.

## 2.6 DETERMINATION OF TOTAL Al BY INDUCTIVELY COUPLED PLASMA ATOMIC EMISSION SPECTROSCOPY (ICP-AES)

The concentration of total aluminum in supernatants was measured by ICP-AES using an Optima 2000 DV Spectrometer (Perking Elmer, Courtabœuf, France) with a 5-points calibration curve (0, 20, 100, 1000, 10 000 ppm). The detection wavelengths for Al were 396.153 nm and 308.215 nm. No dilution was made before analysis.

## 3 THEORY: SURFACE COMPLEXATION MODELING AND INTERFACE DESCRIPTION

The acido-basic properties of the oxide are described in this work using a surface complexation approach with a 2-pK model by equations (1) and (2) with constant  $K_1$  and  $K_2$ , respectively defined as below.



where  $\psi_0$  is the surface potential, depending upon the model chosen to describe the interface,  $F$  is Faraday's constant (96485.309 C.mol<sup>-1</sup>),  $R$  the gas constant (8,31451 J.mol<sup>-1</sup>.K<sup>-1</sup>), and  $T$  the absolute temperature (K), and  $\Delta z$  is the charge changing at the surface. In both equations (1) and (2),  $\Delta z = -1$ . This hypothesis implies that the sites attainable by titration are amphoteric which is not always verified [24].

The constant capacitance model (CCM) is the simplest description of the interface. In this model, acid adsorption is based on a ligand exchange mechanism. All surface complexes are considered inner-sphere complexes and the background electrolyte ions do not form surface complexes, so that the relationship between surface charge ( $\sigma$  in C.m<sup>-2</sup>) and surface potential ( $\psi_0$  in V) is linear [49] :

$$\sigma = C \psi_0 \quad (3)$$

where  $C$  is the capacitance (F.m<sup>-2</sup>) of the system.

Sposito [49] explains that this model cannot be used to describe adsorption as a function of ionic strength and that it should be restricted to specifically adsorbing ions forming inner-

sphere complexes with little dependence on ionic strength. This model was originally restricted to high ionic strength conditions ( $I > 0.1 \text{ mol.L}^{-1}$ ) but Lützenkirchen [50] proposed that it can be also applied to lower ionic strengths. This model requires a low number of adjustable parameters, namely the capacity  $C$ , which is ionic strength dependent, surface site concentration  $N_s$ , and the surface acidity constants  $^{int}K_1$  and  $^{int}K_2$  from reactions (1) and (2).

The double diffuse layer model (DLM) [51,52] describes the interface as composed of a double layer of counter-ions at the surface to compensate surface charge of the particle. The compact layer, closely linked to the surface, and the diffuse layer, where both counter-ions and co-ions are present and the interactions between the ions and the oxide surface are weaker. The diffuse layer does not migrate with the particle. The potential at the compact/diffuse boundary (shear plane) is called  $\zeta$ -potential.

In the framework of the DLM, surface charge of an oxide in a 1:1 electrolyte is given by:

$$\sigma = \sqrt{8 RT \epsilon_R \epsilon_0 I 10^3} \sinh\left(\frac{z F \psi_0}{2 RT}\right) \quad (4)$$

where  $\epsilon_R$  is the relative dielectric constant of the medium (80.2 for water at 293.15 K),  $\epsilon_0$  is the vacuum dielectric constant ( $8.854 \cdot 10^{-12} \text{ C}^2 \cdot \text{N}^{-1} \cdot \text{m}^{-2}$ ),  $z$  is the electrolyte ion charge, and  $I$  is the ionic strength ( $\text{mol.L}^{-1}$ ). Then, expressing  $\sigma$  as a function of the oxide parameters and site concentration leads to:

$$\sigma = \frac{F}{C_s s} \left( [\equiv\text{MOH}_2^+] - [\equiv\text{MO}^-] \right) \quad (5)$$

$$\sigma = \frac{F}{C_s s} [\equiv\text{MOH}] \left( \frac{[\text{H}^+]}{^{int}K_1 \exp\left(\frac{F\psi_0}{RT}\right)} - \frac{^{int}K_2 \exp\left(\frac{F\psi_0}{RT}\right)}{[\text{H}^+]} \right) \quad (6)$$

where  $[\equiv\text{MOH}]$  is site density ( $\text{mol.L}^{-1}$ ),  $s$  is the specific surface area of the oxide ( $\text{m}^2 \cdot \text{g}^{-1}$ ) and  $C_s$  is the oxide concentration ( $\text{g.L}^{-1}$ ).

Rearranging equations (4) and (6), e.g. in the case of the DLM, leads to:

$$\frac{\left( \frac{[\text{H}^+]}{^{int}K_{a1} \exp\left(\frac{F\psi_0}{RT}\right)} - \frac{^{int}K_{a2} \exp\left(\frac{F\psi_0}{RT}\right)}{[\text{H}^+]} \right)}{\left( 1 + \frac{[\text{H}^+]}{^{int}K_{a1} \exp\left(\frac{F\psi_0}{RT}\right)} + \frac{^{int}K_{a2} \exp\left(\frac{F\psi_0}{RT}\right)}{[\text{H}^+]} \right)} = \frac{\sqrt{8 \epsilon_r \epsilon_0 RT I 10^3}}{[\equiv\text{MOH}]} \times \frac{C_s s}{F} \times \sinh\left(\frac{F\psi_0}{2RT}\right) \quad (7)$$

The calculation of the  $\zeta$ -potential from  $\psi_0$  is given in [53] in the DLM framework:

$$\tanh\left(\frac{ze\zeta}{4kT}\right) = \tanh\left(\frac{ze\psi_0}{4kT}\right) \exp(-\kappa x) \quad (8)$$

where  $z$  is the electrolyte ion charge,  $e$  is the elementary charge of electron ( $1.602 \cdot 10^{-19}$  C),  $k$  the Boltzmann constant ( $1.38 \cdot 10^{-23}$  J.K<sup>-1</sup>),  $\kappa$  (nm<sup>-1</sup>) is the reverse Debye length, and  $x$  (nm) is the distance at which  $\zeta$ -potential is measured. Some authors define that distance as the outer Helmholtz plan using the more advanced triple layer model ( $\zeta = \psi_d$ ), but we will adjust this parameter, as well as  $\log_{10}^{\text{int}}K_i$  values, by a trial-and-error approach to minimize the sum of squares. This definition implies that the permittivity is independent of position — or that the properties of water are the same whatever the distance to the surface —, which can be questioned knowing literature values [54], and recent advances on the structure of water at the surface [55].

Practically, the oxide surface charge can be determined either by potentiometric or electrophoretic titrations. The fitting of the data with an appropriate surface complexation model permits to determine the oxide characteristics. Moreover, determining the point of zero charge (PZC) of the oxide is of importance. PZC is the pH at which the surface charge of the oxide is nil. Behind this generic name are several definitions, depending on the authors and experimental method. The evolution of electrophoretic mobility of particles as a function of pH leads to the determination of the isoelectric point (IEP) defined as the pH where the electrophoretic mobility is nil [56]. Potentiometric titrations of the oxide performed at various ionic strengths lead to the determination of the point of zero salt effect (PZSE) [45]. The titration curves are modified according to ionic strength [45,57,58] and the intersection point of these curves is defined as PZSE. For pH = PZSE, the cationic and anionic exchange capacities are equal. For pure oxides, with no specific adsorption, PZSE and IEP should be equal and they can be merged together under the name PZC.

## 4 RESULTS AND DISCUSSION

### 4.1 OXIDE PROPERTIES

The proton induced surface charges of Al<sub>2</sub>O<sub>3</sub> as a function of pH determined by titration are given in Figure 2 for three values of ionic strength, which gives PZSE = 8.5. This value is consistent with data published elsewhere for low carbonated surfaces as shown in Table 2, where the PZSE values range from 7.5 to 9.6 for aluminum oxide. It is worth noting that the compiled PZSE values in Kosmulski [64,65] are in the range from 7.6 to 9.4 (not all reported in Table 2).

During potentiometric titration, increasing ionic strength resulted in increasing surface charge for pH < PZSE. Figure 2 shows that between pH 7 and 9.5 the influence of ionic strength is small and the curves are mostly linear. Out of this pH range, the slopes increase sharply with ionic strength and especially at high pH (data not shown), as already presented for pyrogenic alumina [66] and for gibbsite [45]. Neither downward, at low pH, nor upward, at high pH, curvatures due to extensive solubilisation of the mineral were observed under our conditions.

Table 2. Point of zero salt effect (PZSE) or isoelectric point (IEP) and site densities determined by other authors for various aluminum oxides.

Oxide	PZSE/IEP	Site density (site.nm <sup>-2</sup> )	Reference
$\gamma$ -Al <sub>2</sub> O <sub>3</sub>	8.5 (PZSE)	n.m.	[52]
$\gamma$ -Al <sub>2</sub> O <sub>3</sub>	8.7 (PZSE)	1.3	[21]
$\alpha$ -Al <sub>2</sub> O <sub>3</sub>	9.0 (PZSE)	1.2	[59]
$\gamma$ -Al <sub>2</sub> O <sub>3</sub>	8.6 (PZSE)	1.0	[38]
Al <sub>2</sub> O <sub>3</sub>	7.5 (PZSE)	n.m.	[60,61]
$\alpha$ -Al <sub>2</sub> O <sub>3</sub>	9.1 (PZSE)	1.3	[62]
$\alpha$ -Al <sub>2</sub> O <sub>3</sub>	9,4 (PZSE)	8 <sup>a</sup>	[63]
Commercial Gibbsite	5.4-6.3 (PZSE)	n.m.	[45]
$\alpha$ -Al <sub>2</sub> O <sub>3</sub>	9.2 (IEP)	2.56	[26]
$\alpha$ -Al <sub>2</sub> O <sub>3</sub>	7.2 (IEP)	n.m.	[28]
$\alpha$ -Al <sub>2</sub> O <sub>3</sub>	6.7 (IEP)	n.m.	[30]
Laboratory made gibbsite	11.3 (IEP)	n.m.	[45]
Commercial gibbsite	9 - 9.6 (IEP)	n.m.	[45]

a: from crystallographic data; n.m.: not mentioned in the original text

From the potentiometric titration data, the fit is in very good agreement with the experimental data,  $^{int}K_1$ ,  $^{int}K_2$ , and  $N_s$ , achieved in the framework of the CCM. Due to the large linear part of the titration results, the fitting with DLM cannot converge. As some authors used this model at ionic strengths lower than 0.1 mol.L<sup>-1</sup> [35,67-69], Lützenkirchen [50] stressed that some precautions must be taken so that this model makes sense under low ionic strength conditions. First, the relationship between the oxide charge (or sorbed H<sup>+</sup>) and pH must be linear, which is verified in this work for our values of ionic strength, as shown in Figure 2. Second, the capacitance value must be as low as possible and should theoretically respect,

$$C < 2.28 \sqrt{I} \quad (9)$$

Nevertheless, Lützenkirchen [50] indicated that in low ionic strength media, the capacitance values are almost always higher, making their physical sense doubtful. The authors also explained that increasing site density sometimes permits to reach correct capacitance values, but one should pay attention that the site density remains physically reasonable, i.e. lower than crystallographic determination — see e.g. ref. [70,71].

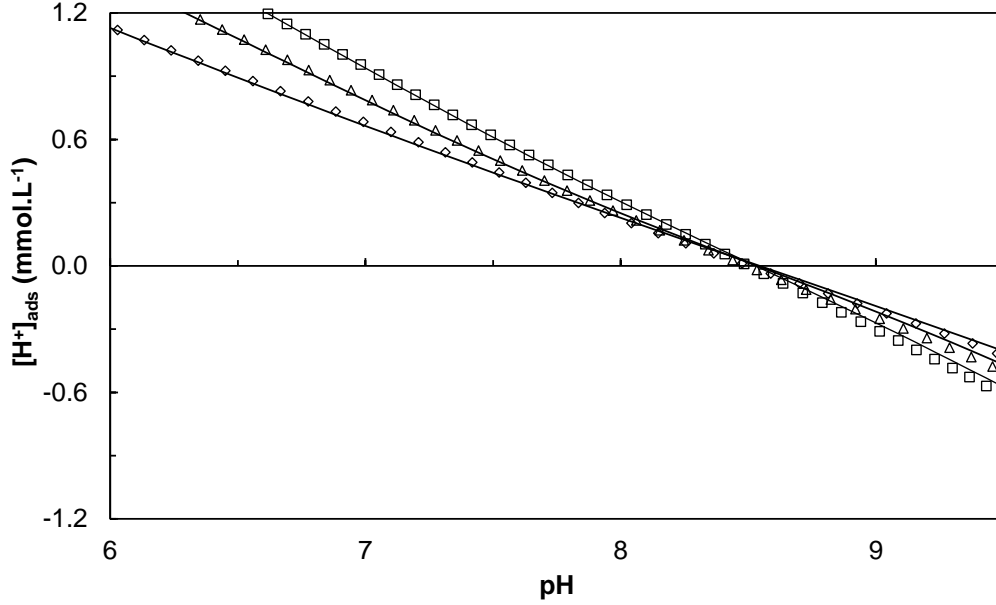


Figure 2. Evolution of the proton induced surface charge of commercial  $\gamma,\alpha\text{-Al}_2\text{O}_3$  during titration:  $C_{\text{Al}_2\text{O}_3} = 10 \text{ g.L}^{-1}$ ,  $I = 0.01 \text{ mol.L}^{-1}$  (diamonds),  $0.1 \text{ mol.L}^{-1}$  (triangles) and  $0.25 \text{ mol.L}^{-1}$  (squares) NaCl; titrant,  $0.1 \text{ mol.L}^{-1}$  NaOH; added volumes,  $10 \mu\text{L}$ ; waiting time between two additions of titrant, max 5 min; fitted curves using CCM, plain lines.

The fitted parameters for the potentiometric titrations are given in Table 3. The adequacy of the fitting procedure, as expressed by the ratio WSOS/D, is satisfactory. The obtained site density is of the same order of magnitude as published elsewhere [21,26,38] and lower than typical values obtained from crystallographic data [70,71]. For the three ionic strengths, the optimized  $C$  values do not satisfy condition (9) (see Figure 3), but they are of the same order of magnitude or lower than those used by other authors in low ionic strength conditions [35,66-69,72].

Table 3: Fitted parameters determined using the CCM, for potentiometric titrations of  $\text{Al}_2\text{O}_3$ :  $I$ , ionic strength ( $\text{mmol.L}^{-1}$ );  $\text{p}K_w$ , water ionic product calculated for each ionic strength using Davies equation;  $C$  capacitance ( $\text{F.m}^{-2}$ );  $\log \text{int}K_1$ ,  $\log \text{int}K_2$ , surface acidity constants (defined in equations 1 and 2);  $d$ , site density (in  $\text{nm}^{-2}$ ); and WSOS/D, accuracy parameter of the fit. The mean values (MEAN) and the uncertainty (UNCERT) calculated by the software are also given.

$I (\text{mmol.L}^{-1})$	$2,28.\sqrt{I}$	$\text{p}K_w$	$C (\text{F.m}^{-2})$	WSOS/D	$\log_{10} \text{int}K_1$	$\log_{10} \text{int}K_2$	$N_s (\text{site.nm}^{-2})$
10	0.23	13.9	0.90	2.36	-7.40	-9.69	2.55
100	0.72	13.8	1.55	3.47	-7.50	-9.57	1.24
250	1.14	13.6	1.75	1.37	-7.56	-9.49	1.45
MEAN					-7.5	-9.6	1.7
UNCERT					0.1	0.6	0.7

As shown in Table 3,  $\text{int}K_1$ ,  $\text{int}K_2$  and  $N_s$  do not vary with ionic strength. Lützenkirchen [50] also remarked a possible linear relationship between  $C$  and  $\log_{10}I$ , as well as between  $\log_{10} \text{int}K_i$  and  $\log_{10}I$ . In our case, this linear relationship seems to be verified for  $C$  and  $\log_{10}I$ , as shown in Figure 3. These results partly validate the use of the CCM for our adsorption studies in the

range  $10 < I \text{ (mmol.L}^{-1}\text{)} < 250$ , at least from an operational point of view, and under the limits defined in this discussion.

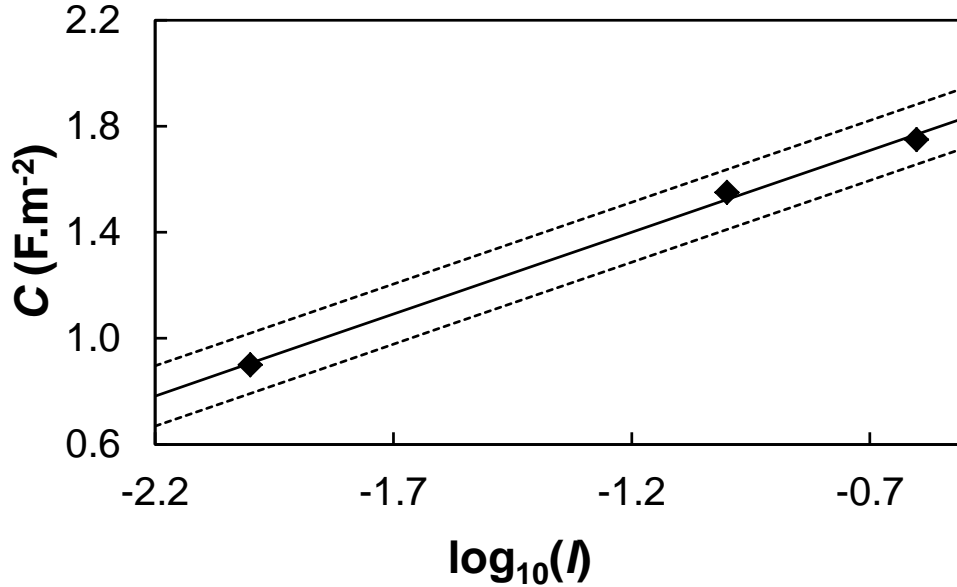


Figure 3. Fitted capacitance value ( $F.m^{-2}$ ) as a function of logarithm of ionic strength. Experimental conditions, see Figure 2, dashed line is the 95% confidence interval.

Electrophoretic mobilities of  $Al_2O_3$  particles were determined at ionic strengths 0.01 and 0.05  $mol.L^{-1}$  NaCl (Figure 4). The electrophoretic data were fitted using the DLM to determine the acido-basic constants of the oxide; using CCM has no meaning for electrophoretic mobility. Surface potential  $\psi_0$  can be estimated from the electrophoretic measurements. The electrophoretic mobility of a particle is representative of the potential at the shear plane ( $\zeta$ -potential), which is approximately located at the boundary between the compact and the diffuse layers. Electrophoretic mobilities are related to  $\zeta$ -potential using Henry's equation (10), assuming no relaxation effect [73]:

$$\mu_{ep} = \frac{2 \zeta \epsilon_R}{3 \eta} f(\kappa r) \quad (10)$$

where  $\eta$  is the viscosity, and  $r$  is the particle radius. Henry's function  $f(\kappa r)$  is monotonously varying with the  $\kappa r$  product and takes values from 1 to 1.5 when  $\kappa r$  varies from 0 to the infinite, respectively. The reverse Debye length  $\kappa^{-1}$  is calculated by,

$$\kappa^{-1} = \sqrt{\frac{\epsilon_0 \epsilon_R R T}{F^2 I}} \quad (11)$$

where  $R$  is the gas constant ( $8.31451 \text{ J mol}^{-1} \text{ K}^{-1}$ ),  $F$  is the Faraday constant ( $96485.309 \text{ C mol}^{-1}$ ),  $I$  is the ionic strength of the solution ( $mol.dm^{-3}$ ). For liquid water at  $20^\circ\text{C}$ ,  $\epsilon_R = 80.2$  and  $\eta = 1.002 \text{ mPa.s}$ , so that,

$$\kappa^{-1} \approx \frac{0.305}{\sqrt{I}} \text{ (nm)} \quad (12)$$

and the  $\kappa^{-1}$  values are 3.05 and 1.36 nm, respectively.

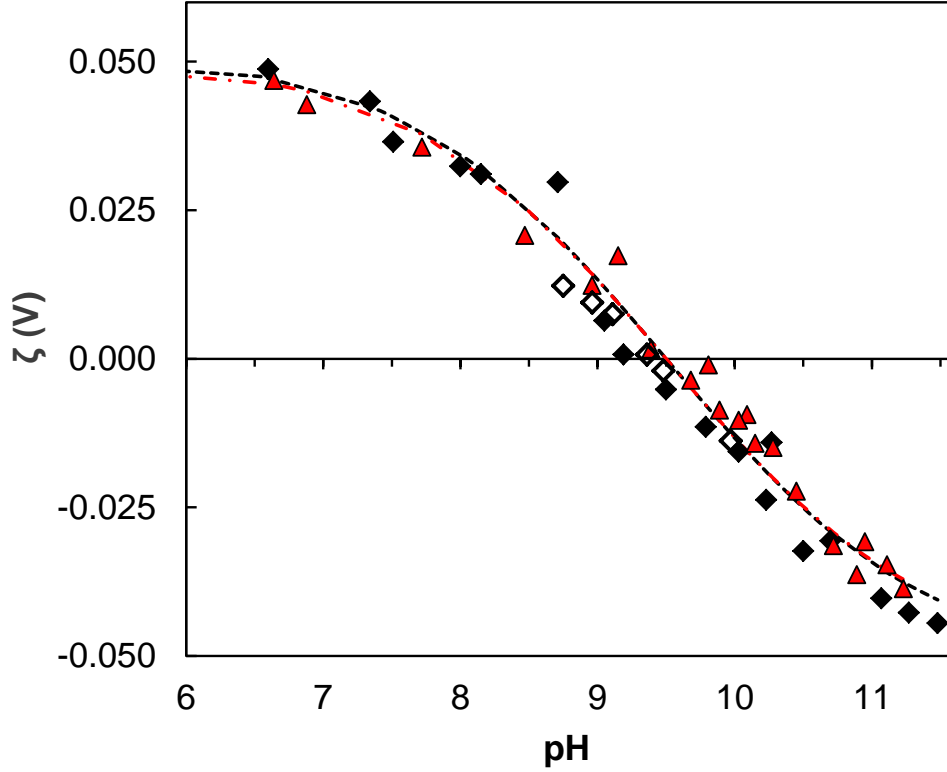


Figure 4. Experimental  $\zeta$ -potential (V) of  $\alpha,\gamma$ - $\text{Al}_2\text{O}_3$  particles vs. pH calculated from mobility measurement (see text for details):  $C_{\text{Al}_2\text{O}_3} = 0.5 \text{ g.L}^{-1}$ ,  $I = 0.05 \text{ mol.L}^{-1}$  NaCl (red triangles) and  $0.01 \text{ mol.L}^{-1}$  NaCl (open and filled diamonds, representing two stock suspensions of  $\text{Al}_2\text{O}_3$ ); total sample volume 100 mL; volume of each analyzed sample, 200  $\mu\text{L}$ ; titrant,  $1 \text{ mol.L}^{-1}$  HCl or NaOH; maximum waiting time between 2 additions of titrant, 5 min; the error bars are covered by the symbol size; dashed line, adjusted  $\zeta$ -potential for  $0.01 \text{ mol.L}^{-1}$  NaCl; dash-dot line, adjusted  $\zeta$ -potential for  $0.05 \text{ mol.L}^{-1}$  NaCl.

Ohshima [74] proposed an approximated expression for Henry's function, valid for all  $\kappa r$  values and inducing a systematic error inferior to 1%,

$$f(\kappa r) = 1 + \frac{1}{2 \left(1 + \frac{\delta}{\kappa r}\right)^3} \quad (13)$$

where  $\delta$  is calculated using:

$$\delta = \frac{2.5}{1 + 2 \exp(-\kappa r)} \quad (14)$$

Equations (10) to (14) permit to convert experimental electrophoretic mobility into an experimental  $\zeta$ -potential ( $\zeta_{\text{exp}}$ ). Equations (7) and (8) were used to determine a calculated  $\zeta$ -potential ( $\zeta_{\text{calc}}$ ). The values  $^{\text{int}}K_1$  and  $^{\text{int}}K_2$  were determined by minimizing the sum of squares between  $\zeta_{\text{exp}}$  and  $\zeta_{\text{calc}}$ , using the value of  $N_s$  determined in potentiometry. The best fit yields  $\log_{10}^{\text{int}}K_1 = -8.9$ ,  $\log_{10}^{\text{int}}K_2 = -10.1$ , which yields in IEP = 9.5, and  $x$  values are 2.3 (75%  $\kappa^{-1}$ ) and 1.05 (77%  $\kappa^{-1}$ ) nm for 0.01 and 0.05 mol.L<sup>-1</sup>, respectively.

The IEP value determined in this work is within the range of data reported by others [26,45] (see Table 2) and with compilation of data [64,65,75]. As presented in Figure 4, changing ionic strength in the range 10-50 mmol.L<sup>-1</sup> impacts only very slightly the electrophoretic mobility of particles, and the IEP does not significantly depend on ionic strength under these conditions. It was not possible to work under higher ionic strength because of Joule effect in the zetameter cell, despite the use of a low voltage (50 V) and of a special cell (ZEN 1010, Malvern) designed for high concentration suspensions. Moreover, Naveau *et al.* [57] mentioned the difficulty to measure electrophoretic mobility of particles for pH close to the PZC because of flocculation and aggregation at this pH. This, however, was not observed in this study.

There is a significant difference between obtained IEP 9.5 and PZSE 8.5. Such a difference was scarcely already reported for Al(III) and Fe(III) oxides [45,49,58,68,70]. It could be attributed to the presence of side reactions during titration, e.g. specific adsorption of the electrolyte, dissolution, precipitation, hydrolysis of aluminum species (for example the formation of polynuclear complexes of aluminum), influence of surface impurities, and defects on the oxide surface [45] but these processes are not much documented. The presence of an initial surface charge at the beginning of potentiometric titration may also lead to a slight difference [46].

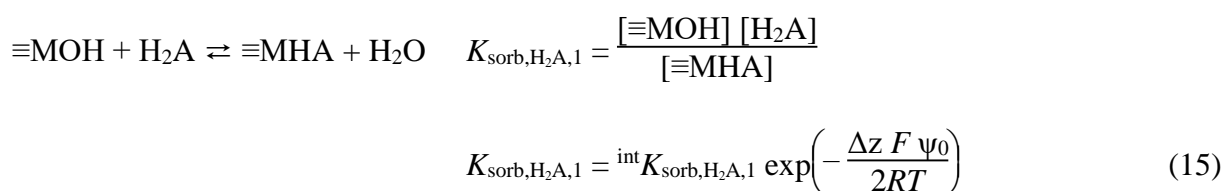
IEP and PZSE values are different when electrolyte ions adsorb specifically. Wood *et al.* [70] for instance interpreted their results in the framework of the triple layer model [76] with a difference in specific adsorption of the electrolyte ions that is not encountered when IEP and PSZE are the same. Na<sup>+</sup> and Cl<sup>-</sup> are used in our work as background ions during potentiometric titrations and electrophoretic measurements. Parks [77] proposed that Na<sup>+</sup> do not sorb specifically onto Al<sub>2</sub>O<sub>3</sub>, meaning that its adsorption onto Al<sub>2</sub>O<sub>3</sub> particles is reversible. Similarly, Alliot *et al.* [24] showed that Na<sup>+</sup> did not sorb significantly onto  $\alpha$ -Al<sub>2</sub>O<sub>3</sub> at pH 5 whereas Cl<sup>-</sup> does. On the contrary, Adekola *et al.* [45] suggested that Na<sup>+</sup> sorbs onto Al<sub>2</sub>O<sub>3</sub>, shifting the IEP to higher values. These authors performed several titrations using potentiometry and electrophoretic mobility measurements on two gibbsite samples (commercial and laboratory made). Their study was carried on in different laboratories and with different experimental parameters such as ionic strength, salt composition, volume of titrant and time interval between two added aliquots. The range for PZSE values (5.4–6.3) between the various laboratories and experimental conditions is wider than the range for IEP values (9.0-9.6).

As a rationale, the difference observed in the present study between IEP and PZSE is most probably due to the heterogeneity of the oxide, either phase heterogeneity, as this oxide is made of  $\gamma$ - and  $\alpha$ -Al<sub>2</sub>O<sub>3</sub>, or because of the presence of impurities, or of the background electrolyte ions. As the objective of this work is not the intimate description of the composite material, we will use the simplest model CCM to obtain reasonably sound parameters in an operational view.

## 4.2 CONSTANT-pH ISOTHERMS OF PHENOLIC ACIDS ONTO $Al_2O_3$

The constant-pH isotherms at pH 5 from  $H_2Phb$  and  $H_2Proto$  are reported on Figure 5. The increase of adsorption when adding one distal phenolic group is evident. The results  $H_2Proto$  and  $H_2Gal$  (Figure 6) onto the mineral are very similar except that adsorption of  $H_2Gal$  clearly exhibit two plateaus, which is not so clear for  $H_2Proto$ . This point will be discussed in the following.

Figure 5 shows the experimental data and the fitting curve for adsorption of  $H_2Phb$  and  $H_2Proto$  using the oxide parameters previously determined in the framework of the CCM. It is clear that adsorption of  $H_2Phb$  is not influenced by alumina concentration in the range of alumina concentration  $0.5\text{-}5\text{ g.L}^{-1}$ . In this first fitting procedure only one surface species was considered, even for adsorption of  $H_2Proto$ . The following surface reaction [78], was considered:



where  $H_2A$  stands for the studied phenolic acid figuring only its two lower  $pK_a$ s; here  $\Delta z = 0$  and Boltzmann factor is unity.

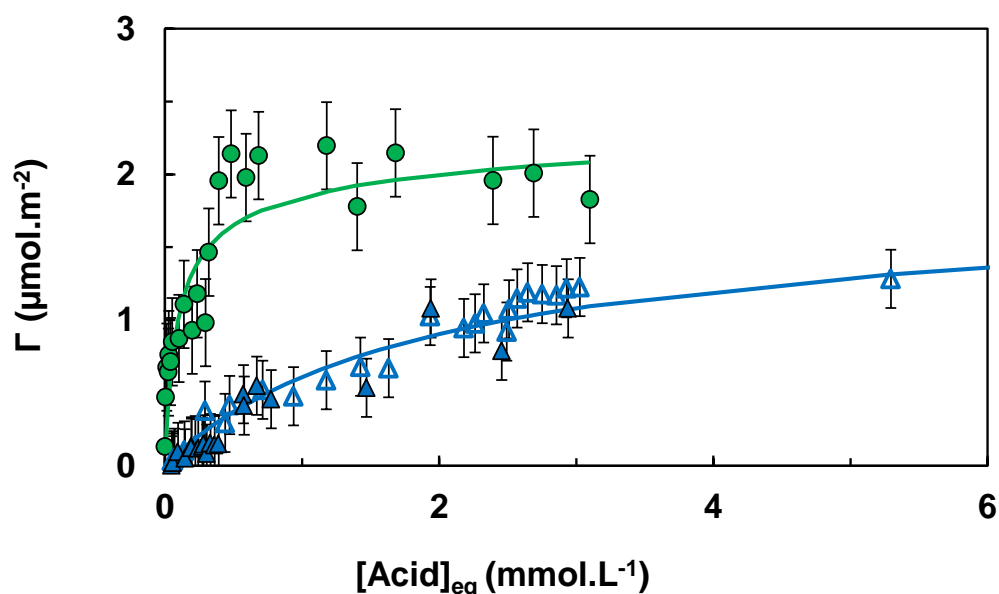


Figure 5. Constant-pH isotherms of  $H_2Phb$  and  $H_2Proto$  onto aluminum oxide,  $I = 0.01\text{ mol.L}^{-1}$  NaCl, pH 5.0: green circles,  $H_2Proto$ ,  $C_{Al_2O_3} = 0.5\text{ g.L}^{-1}$ ; open triangles,  $H_2Phb$ ,  $C_{Al_2O_3} = 5\text{ g.L}^{-1}$ ; filled triangles,  $H_2Phb$ ,  $C_{Al_2O_3} = 0.5\text{ g.L}^{-1}$ ; plain lines represent fitted curves obtained with the CCM. The error bars represent experimental uncertainty.

Based on a aluminol site density of  $1.7\text{ site.nm}^{-2}$ , the saturation plateaus obtained in Figure 5 correspond to  $\approx 52\%$  and  $\approx 68\%$  of this density for the cases of  $H_2Phb$  and  $H_2Proto$ ,

respectively. At pH 5, the adsorption constant ( $\log_{10}^{\text{int}}K_{\text{sorb,H}_2\text{A},1}$ ) for H<sub>2</sub>Proto determined with FITEQL using equation (15) is one and a half time higher than that for H<sub>2</sub>Phb (Table 4). Adsorption capacities for H<sub>2</sub>Phb from this work (see Table 4) are in fair agreement with otherwise published data [25,30]. For H<sub>2</sub>Proto the situation is slightly more intricate as Borah *et al.* [31] limited their study in the range of equilibrium concentration of  $[\text{H}_2\text{Proto}]_{\text{eq}} \leq 0.2$  mmol/L and found  $\Gamma_{\text{max}} = 1 \mu\text{mol}/\text{m}^2$ . Under our conditions, the maximum equilibrium concentration 3 mmol/L, but a closer inspection of our results shows that at  $[\text{H}_2\text{Proto}]_{\text{eq}} = 0.2$  mmol/L,  $\Gamma \cong 1 \mu\text{mol}/\text{m}^2$ .

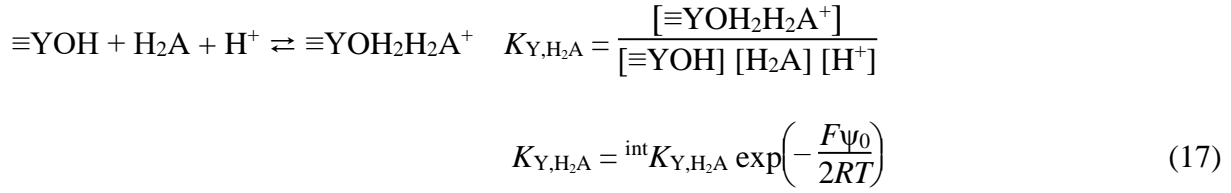
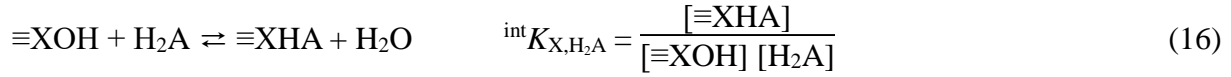
Table 4: Sorption characteristics for H<sub>2</sub>Phb and H<sub>2</sub>Proto/oxide systems from this work and published data considering one surface species.

Acid	Oxide	$\log_{10}^{\text{int}}K_{\text{sorb,H}_2\text{A},1}$	$\Gamma_{\text{max}}$ ( $\mu\text{mol}\cdot\text{m}^{-2}$ )	pH	$I$ ( $\text{mmol}\cdot\text{L}^{-1}$ ) - medium	Model	Ref
H <sub>2</sub> Phb	Al <sub>2</sub> O <sub>3</sub>	0.4	1.8	5	0.5-NaCl	Langmuir	[30]
H <sub>2</sub> Phb	Fe <sub>2</sub> O <sub>3</sub>	2.9	1.2	5.5	50-NaClO <sub>4</sub>	Langmuir	[25]
H <sub>2</sub> Phb	Al <sub>2</sub> O <sub>3</sub>	$3.4 \pm 0.1$	$1.8 \pm 0.1$	5	10-NaCl	CCM	this work
H <sub>2</sub> Proto	Al <sub>2</sub> O <sub>3</sub>	1.8	1.1	5	0.5-NaCl	Langmuir	[31]
H <sub>2</sub> Proto	Al <sub>2</sub> O <sub>3</sub>	$5.4 \pm 0.1$	$2.0 \pm 0.1$	5	10-NaCl	CCM	this work

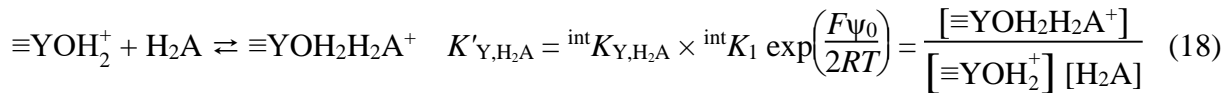
The lower adsorption constant determined for H<sub>2</sub>Phb as compared to H<sub>2</sub>Proto is consistent with the work by Das *et al.* [30] — in the framework of a different modelling —, who showed, using diffuse reflectance infrared Fourier-transformed spectroscopy, that OH<sub>phen</sub> of H<sub>2</sub>Phb is not involved in adsorption onto Al<sub>2</sub>O<sub>3</sub> and that the complex formed is outer-sphere at pH 5. Guan *et al.* [33] also argued that the presence of two adjacent OH groups on the aromatic ring increases adsorption, as it creates a second adsorption possibility, in a chelate mode. Indeed, Guan *et al.* [33] and Borah *et al.* [31] showed using ATR-FTIR, that OH<sub>phen</sub> is involved in surface complexation of H<sub>2</sub>Proto onto Al<sub>2</sub>O<sub>3</sub>, as pH increases. As a consequence, the implication of OH<sub>phen</sub> for adsorption of H<sub>2</sub>Proto could create another adsorption possibility that does not exist in H<sub>2</sub>Phb involving the catechol group. Moreover, Hidber *et al.* [26] showed that increasing the number of OH<sub>phen</sub>, lead to increasing adsorption onto Al<sub>2</sub>O<sub>3</sub> between pH 4 and 10. But these authors worked with molecules in which the carboxylate and one phenolate are adjacent functional group on the aromatic ring (which is not the case in this study). However the same conclusion seems to be drawn here, even if the phenolate and carboxylate groups are not adjacent on the aromatic ring.

Adsorption of H<sub>2</sub>Gal onto Al<sub>2</sub>O<sub>3</sub> was also fitted using CCM parameters of Al<sub>2</sub>O<sub>3</sub>, but considering that two surface sites are available for H<sub>2</sub>Gal, and that the acidities of both sites have the same protolytic properties because only one amphoteric site was evidenced by potentiometric titration. It can be argued that some sites may not be evidenced during titration, as doubly coordinated sites  $\equiv\text{X}_2\text{OH}$  [71]. Nevertheless, Yoon *et al.* [79] evidenced at least four sorption mechanism for oxalate on  $\alpha$ -Al<sub>2</sub>O<sub>3</sub> and boehmite depending on acid concentration.

Thus the following two surface reactions were considered:



The latter equilibrium could be rewritten without a change in the surface charge:



The fitted curve, given in Figure 6 leads to  $\log_{10}K_{\text{X,H}_2\text{Gal}} = 3.6 \pm 0.1$  and  $\log_{10}K_{\text{Y,H}_2\text{Gal}} = 15.5 \pm 0.7$ , is not totally satisfactory especially for the highest concentration of  $\text{H}_2\text{Gal}$ . A further fitting can be done using the number of adsorption sites as an adjustable parameter, which yields in a greater number of adsorption sites than determined by titration. This would mean that there are a certain number of sites, which were not evidenced during titration experiment that participates to the fixation of  $\text{H}_2\text{Gal}$ . This assumption is not possible to ascertain within the framework of this study but recalls the low number of accessible sites in titration compared to crystallographic sites [71].

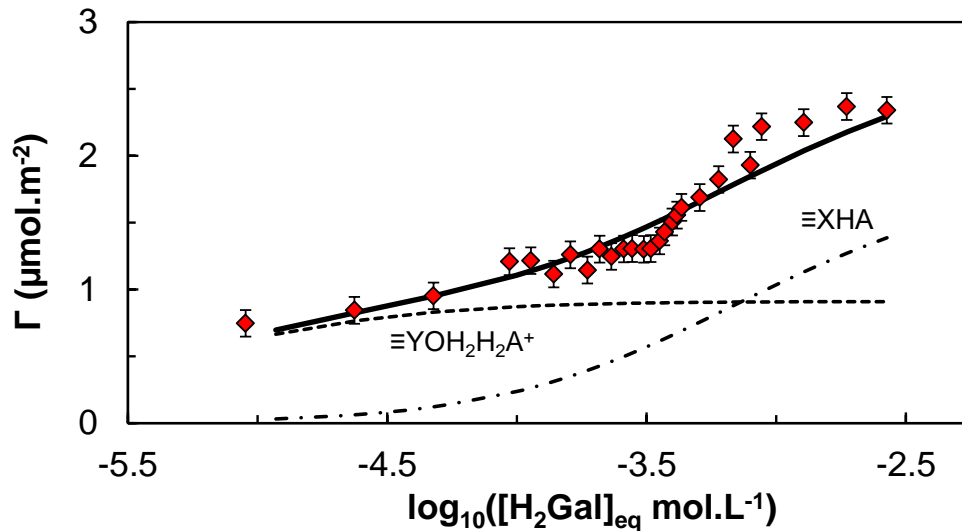


Figure 6. Constant-pH isotherm of  $\text{H}_2\text{Gal}$  onto  $\text{Al}_2\text{O}_3$  (red diamonds) and fitted curve using obtained with FITEQL software in the framework of the CCM parameters for  $\text{Al}_2\text{O}_3$  (plain line).  $I = 0.01 \text{ mol.L}^{-1}$  NaCl, pH 5,  $C_{\text{Al}_2\text{O}_3} = 0.5 \text{ g.L}^{-1}$ . The error bars represent experimental uncertainty.

The experimental data obtained for  $\text{H}_2\text{Proto}$  were also fitted using two adsorption sites and two surface species. The results for  $\text{H}_2\text{Proto}$  are given in Figure 7 and lead to  $\log_{10}^{\text{int}}K_{\text{X,H}_2\text{Proto}} = 3.95 \pm 0.1$  and  $\log_{10}^{\text{int}}K_{\text{Y,H}_2\text{Proto}} = 15.9 \pm 0.7$ , but is not completely satisfactory. For both  $\text{H}_2\text{Proto}$

and H<sub>2</sub>Gal, the constants determined for species ≡XAH are very close to that determined previously for H<sub>2</sub>Phb (see Table 4). The reason for the implication of two surface sites in the case of adsorption of H<sub>2</sub>Gal, and eventually H<sub>2</sub>Proto was out of the range of this study but would require further developments.

As our objective is the sufficiently sound modeling of our system in an operational view, the simplest modelings may be used.

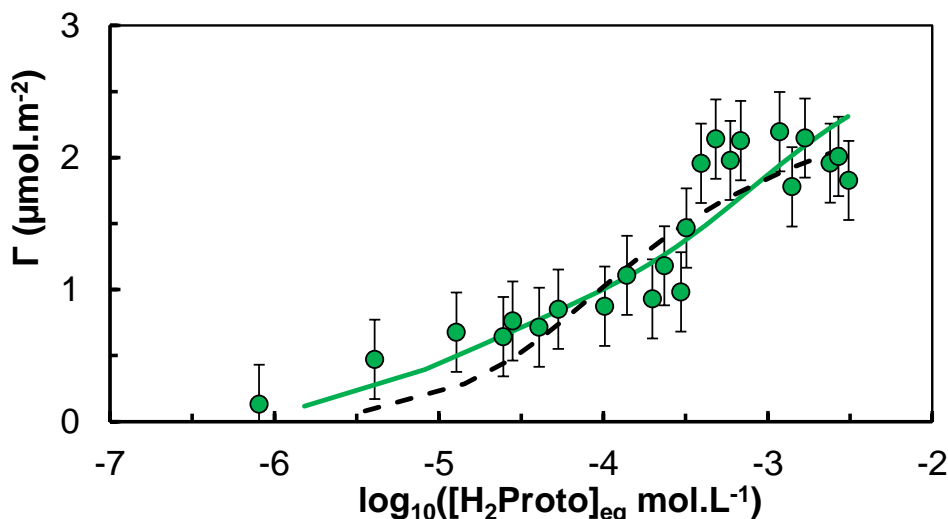
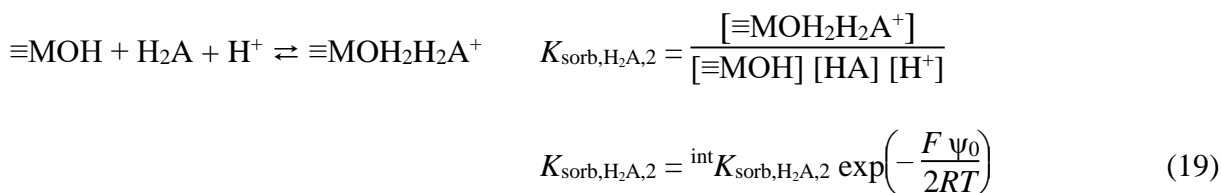


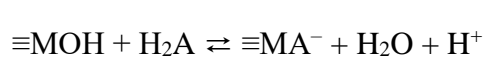
Figure 7. Constant-pH isotherm of H<sub>2</sub>Proto onto Al<sub>2</sub>O<sub>3</sub> (green circles) and fitted curves for the one site (dashed line from Figure 5) and the two sites (plain line) hypotheses obtained using CCM parameters for Al<sub>2</sub>O<sub>3</sub>;  $I = 0.01 \text{ mol.L}^{-1}$  NaCl, pH 5.0,  $C_{\text{Al}_2\text{O}_3} = 0.5 \text{ g.L}^{-1}$ ; the error bars represent experimental uncertainty.

### 4.3 INFLUENCE OF pH ON THE ADSORPTION OF THE PHENOLIC ACIDS ONTO Al<sub>2</sub>O<sub>3</sub>

The adsorption of the acids were also studied at a fixed concentration *vs.* pH. For each acid, this concentration was chosen with respect to the onset of the saturation plateau. It must be stressed here that from a thermodynamic point of view, neither aluminum oxyhydroxyde is supposed to be stable at  $\text{pH} \leq 4$ .

As shown in Figure 8, and in agreement with literature data reported for Al<sub>2</sub>O<sub>3</sub> [26,30] and goethite [23], adsorption of H<sub>2</sub>Phb onto oxides decreases with increasing pH. In addition to previously retained ≡MHPPhb surface species ( $\log K_{\text{sorb,H}_2\text{Phb},1} = 3.4$ ) at pH 5, two other sorbed species were taken into account to fit the data using the CCM:





$$K_{\text{sorb,H}_2\text{A},3} = \frac{[\equiv\text{MA}^-] [\text{H}^+]}{[\equiv\text{MOH}] [\text{H}_2\text{A}]}$$

$$K_{\text{sorb,H}_2\text{A},3} = {}^{\text{int}}K_{\text{sorb,H}_2\text{A},3} \exp\left(\frac{F\psi_0}{2RT}\right) \quad (20)$$

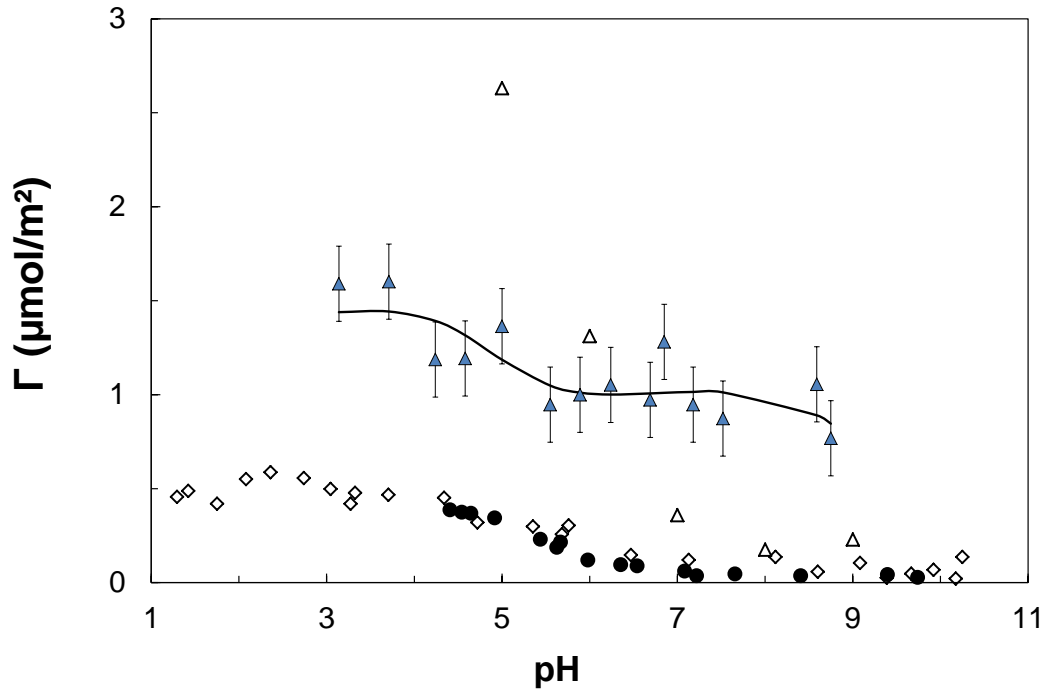


Figure 8. Adsorption of  $\text{H}_2\text{Phb}$  onto Al and Fe oxides as a function of pH from this work (blue triangles,  $C_{\text{Al}_2\text{O}_3} = 0.5 \text{ g.L}^{-1}$ ,  $I = 0.01 \text{ mol.L}^{-1}$  NaCl,  $[\text{H}_2\text{Phb}] = 10^{-3} \text{ mol.L}^{-1}$ ), and literature: the plain line represents the fitted curve obtained using the CCM; closed circles,  $C_{\text{Al}_2\text{O}_3} = 60 \text{ g.L}^{-1}$ ,  $I = 0.1 \text{ mol.L}^{-1}$   $\text{KNO}_3$ ,  $[\text{H}_2\text{Phb}] = 10^{-3} \text{ mol.L}^{-1}$  [11]; open triangles,  $C_{\text{Al}_2\text{O}_3} = 33 \text{ g.L}^{-1}$ ,  $I = 5 \cdot 10^{-5} \text{ mol.L}^{-1}$  NaCl,  $[\text{H}_2\text{Phb}] = 4.5 \cdot 10^{-3} \text{ mol.L}^{-1}$  [30]; open diamonds,  $C_{\alpha\text{-Fe}_2\text{O}_3} = 2 \text{ g.L}^{-1}$ ,  $I = 0.01 \text{ mol.L}^{-1}$  NaCl,  $[\text{H}_2\text{Phb}] = 0\text{-}4.3 \cdot 10^{-4} \text{ mol.L}^{-1}$  [23].

The fitted parameters were  $\log_{10} {}^{\text{int}}K_{\text{sorb,H}_2\text{A},2}$  and  $\log_{10} {}^{\text{int}}K_{\text{sorb,H}_2\text{A},3}$ ; the other parameters are taken from Table 3 and Table 4. The obtained values for  $\text{H}_2\text{Phb}$  were  $\log_{10} {}^{\text{int}}K_{\text{sorb,H}_2\text{Phb},2} = 10.8 \pm 0.8$  (for  $\equiv\text{MOH}_2\text{H}_2\text{Phb}^+$ ) and  $\log_{10} {}^{\text{int}}K_{\text{sorb,H}_2\text{Phb},3} = -0.1 \pm 0.05$  (for  $\equiv\text{MPhb}^-$ ). The resulting fitted curve is represented in Figure 8 together with literature data. The pH envelope of  $\text{H}_2\text{Proto}$  at a fixed concentration as a function of pH is given in Figure 9 together with literature data for  $\text{H}_2\text{Proto}$  and catechol.

Figure 9 shows that adsorption of  $\text{H}_2\text{Proto}$  remains approximately constant between pH range 3-7, consistently with results obtained for various aluminum and iron oxides [21,23,27,31,80]. Evanko and Dzombak [27] found a maximum adsorption in the pH range 5-7. Contrary to  $\text{H}_2\text{Proto}$ , catechol adsorption increases with pH, because of the implication of the phenolate groups on adsorption, which is very weak below pH 5.

As for  $\text{H}_2\text{Phb}$ , in addition to  $\equiv\text{MHPProto}$  surface species ( $\log K_{\text{sorb,H}_2\text{Proto},1} = 5.4$ ) at pH 5, two other sorbed species must be taken into account to fit the data with FITEQL (*vide supra*). The obtained values for  $\text{H}_2\text{Proto}$  were  $\log K_{\text{sorb,H}_2\text{Proto},2} = 9.2 \pm 0.2$  and  $\log K_{\text{sorb,H}_2\text{Proto},3} = 0.2 \pm 0.1$  for

$\equiv\text{MOH}_2\text{H}_2\text{Proto}^+$  and  $\equiv\text{MProto}^-$ , respectively. Consistently with [26], we show that increasing the number of OH groups on the aromatic ring leads to high adsorption over a wider pH range. Indeed, adsorption of  $\text{H}_2\text{Proto}$  (2 distal  $\text{OH}_{\text{phen}}$ ) remains high over a large pH range (from pH 3 to 7.5), whereas adsorption of  $\text{H}_2\text{Phb}$  (1 distal  $\text{OH}_{\text{phen}}$ ) decreases with pH.

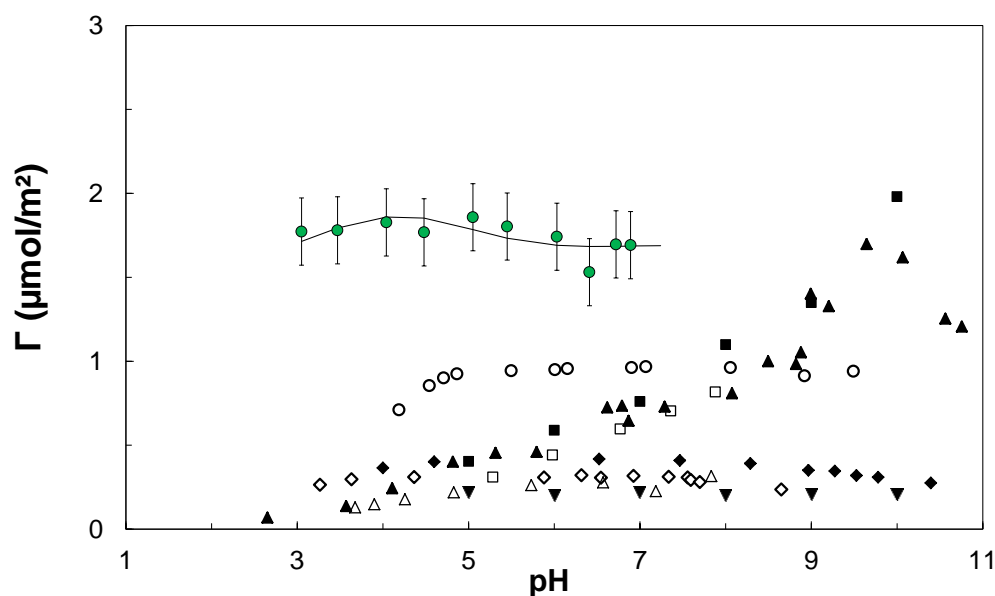


Figure 9. Adsorption of  $\text{H}_2\text{Proto}$  and catechol (1,2 dihydroxybenzene) onto Al and Fe oxides vs. pH from this work (green circles,  $C_{\text{Al}_2\text{O}_3} = 0.5 \text{ g.L}^{-1}$ ,  $I = 0.01 \text{ mol.L}^{-1}$  NaCl,  $[\text{H}_2\text{Proto}] = 8 \cdot 10^{-4} \text{ mol.L}^{-1}$ ) and literature data: plain line represents fitted curve using the CCM; open circles,  $C_{\text{Al}_2\text{O}_3} = 60 \text{ g.L}^{-1}$ ,  $I = 0.01 \text{ mol.L}^{-1}$   $\text{KNO}_3$ ,  $[\text{H}_2\text{Proto}] = 10^{-3} \text{ mol.L}^{-1}$  [11]; inverted closed triangles,  $C_{\text{Al}_2\text{O}_3} = 33 \text{ g.L}^{-1}$ ,  $I = 0.05 \text{ mol.L}^{-1}$  NaCl,  $[\text{H}_2\text{Proto}] = 2 \cdot 10^{-4} \text{ mol.L}^{-1}$  [31]; open diamonds,  $C_{\text{Goethite}} = 1.6 \text{ g.L}^{-1}$ ,  $I = 0.01 \text{ mol.L}^{-1}$  NaCl,  $[\text{H}_2\text{Proto}] = 5 \cdot 10^{-5} \text{ mol.L}^{-1}$  [27]; closed diamonds,  $C_{\text{Goethite}} = 6.9 \cdot 10^{-4} \text{ mol.L}^{-1}$ ,  $I = 0.1 \text{ mol.L}^{-1}$   $\text{NaNO}_3$ ,  $[\text{H}_2\text{Proto}] = 2 \cdot 10^{-5} \text{ mol.L}^{-1}$  [80]; open squares,  $C_{\alpha\text{-Al}_2\text{O}_3} = 2.27 \text{ g.L}^{-1}$ ,  $I = 0.1 \text{ mol.L}^{-1}$   $\text{NaClO}_4$ ,  $[\text{Catechol}] = 0.4 \cdot 10^{-3} \text{ mol.L}^{-1}$  [21]; closed squares,  $C_{\text{Al}_2\text{O}_3} = 33 \text{ g.L}^{-1}$ ,  $I = 0.05 \text{ mol.L}^{-1}$  NaCl,  $[\text{Catechol}] = 4 \cdot 10^{-4} \text{ mol.L}^{-1}$  [31]; closed triangles,  $C_{\alpha\text{-Fe}_2\text{O}_3} = 2 \text{ g.L}^{-1}$ ,  $I = 0.01 \text{ mol.L}^{-1}$  NaCl,  $[\text{Catechol}] = 0\text{--}4.3 \cdot 10^{-4} \text{ mol.L}^{-1}$  [23]; open triangles,  $C_{\text{Goethite}} = 1.6 \text{ g.L}^{-1}$ ,  $I = 0.01 \text{ mol.L}^{-1}$  NaCl,  $[\text{Catechol}] = 5 \cdot 10^{-5} \text{ mol.L}^{-1}$  [27].

In this study, it was not possible to work with pH higher than 7.5 with  $\text{H}_2\text{Proto}$ , because an irreversible chemical change occurred above this pH. Binary systems containing  $\text{H}_2\text{Proto}$  were stirred for 3 days, centrifuged and all the supernatants of samples equilibrated at  $\text{pH} > 7.5$  were irreversibly brown colored and the UV-vis spectra of supernatant were modified. These changes could be attributed to complexation with dissolved aluminum or to degradation to  $\text{H}_2\text{Proto}$  with increasing pH, as it is the case for  $\text{H}_2\text{Gal}$  [81-83]. Indeed, it was also shown that  $\text{H}_2\text{Proto}$  could be degraded upon exposition to  $\text{H}_2\text{O}_2$ , dissolved  $\text{O}_2$ , or UV light [84].

Adsorption of  $\text{H}_2\text{Gal}$  was also studied as a function of pH, for a fixed acid concentration, as shown in Figure 10. It can be seen that adsorption of  $\text{H}_2\text{Gal}$  does not vary significantly as a function of pH between pH 3.5 and 7, as reported by Evanko and Dzombak for goethite [27]. However, it is difficult to evidence a clear trend as data dispersion is high and as  $\text{H}_2\text{Gal}$  is degraded at pH higher than 6.5.

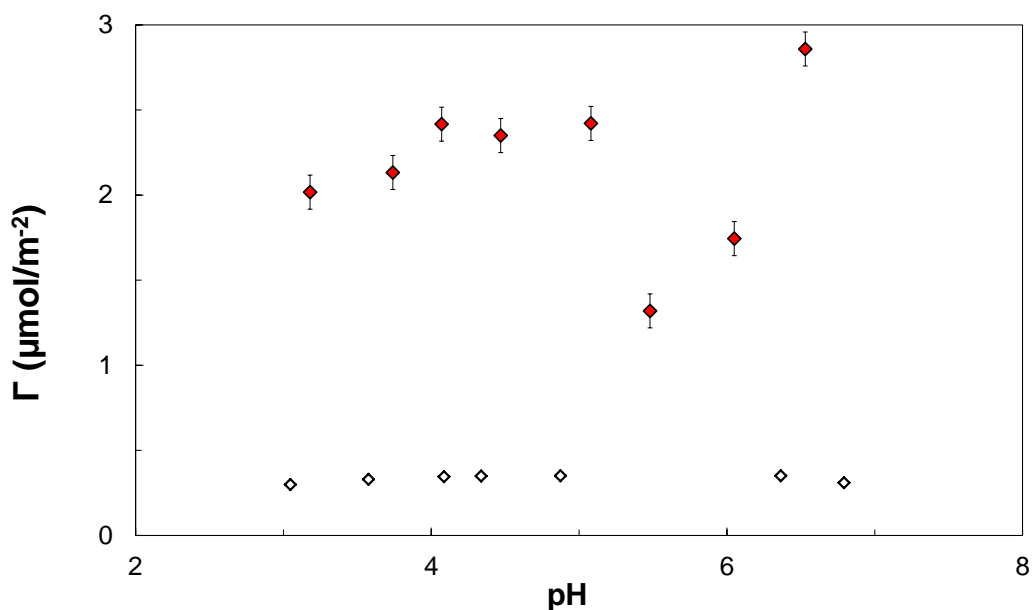


Figure 10. Adsorption of H<sub>2</sub>Gal onto Al and Fe oxides as function of pH: red diamonds, this work,  $C_{\text{Al}_2\text{O}_3} = 0.5 \text{ g.L}^{-1}$ ,  $I = 0.01 \text{ mol.L}^{-1}$  NaCl,  $[\text{H}_2\text{Gal}] = 10^{-3} \text{ mol.L}^{-1}$ ; open diamonds,  $C(\text{goethite}) = 1.6 \text{ g.L}^{-1}$ ,  $I = 0.01 \text{ mol.L}^{-1}$ ,  $[\text{H}_2\text{Gal}] = 5 \cdot 10^{-5} \text{ mol.L}^{-1}$  [27]. The error bars represent experimental uncertainty.

#### 4.4 INFLUENCE OF THE PHENOLIC ACIDS ON THE MINERAL SOLUBILITY

The chosen phenolic acids complex metallic cations [1,83] and can thus dissolve a mineral. The dissolution of the mineral at pH 5 in the presence of a phenolic acid was estimated by determining the concentration of total aluminum by ICP-AES in the supernatant after centrifugation. The evolution of  $C_{\text{Al,diss}}$  vs. concentration of phenolic acid at pH 5 — under carboxylate form — is given in Figure 11, together with theoretical dissolutions for different Al<sub>2</sub>O<sub>3</sub> phases the thermodynamic constants in Table 1 and the experimental mineral dissolution when no ligand is added.

Dissolution of aluminum oxo-hydroxides are low in the neutral pH region whereas it is higher for pH below 5 or above 8 [11,13,47,69]. Figure 11 shows that experimental dissolution without acid at pH 5 is of the same order of magnitude as that calculated for  $\alpha$ -Al<sub>2</sub>O<sub>3</sub> and bayerite, and lower than that calculated for  $\gamma$ -Al<sub>2</sub>O<sub>3</sub>. As awaited from thermodynamic data, Carrier *et al.* [47] showed that  $\gamma$ -Al<sub>2</sub>O<sub>3</sub> surface is not stable with time –  $\gamma$ -Al<sub>2</sub>O<sub>3</sub> is a high temperature phase. They showed that a bayerite phase was formed at the mineral surface. As an equilibration time of 7 days was used in our study, a change in the repartition of phases in the material can be awaited and the solubility limiting phase may not be the major  $\gamma$ -Al<sub>2</sub>O<sub>3</sub>.

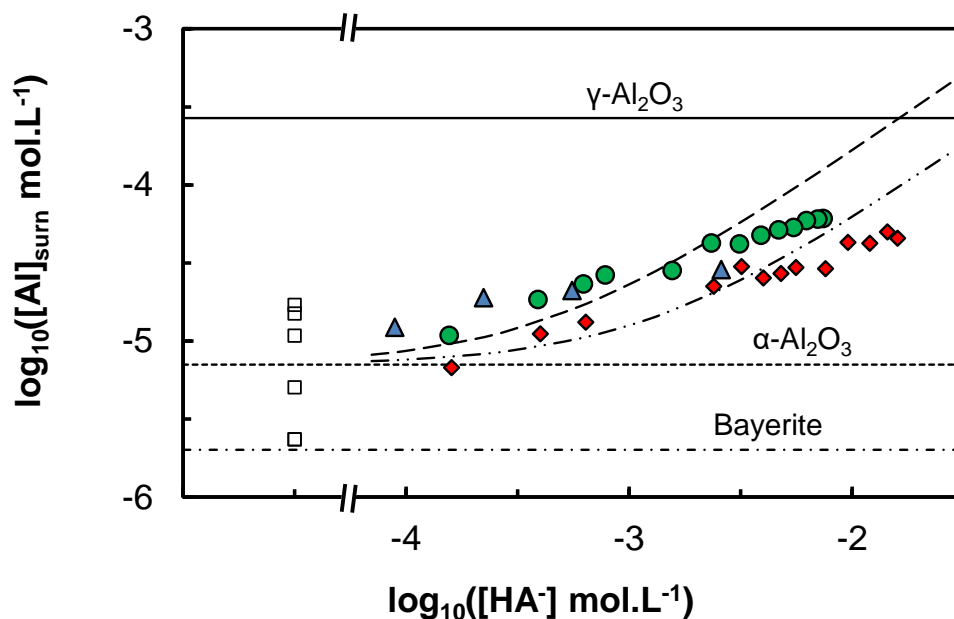


Figure 11. Evolution of aluminium solubility in supernatants when no ligand is added (open squares), and vs. acid concentration for H<sub>2</sub>Phb (blue triangles), H<sub>2</sub>Proto (green circles), and H<sub>2</sub>Gal (red diamonds),  $C_{\text{Al}_2\text{O}_3} = 0.5 \text{ g.L}^{-1}$  and  $I = 0.01 \text{ mol.L}^{-1}$  NaCl, pH 5.0. The theoretical curve calculated for  $\gamma\text{-Al}_2\text{O}_3$  (plain line),  $\alpha\text{-Al}_2\text{O}_3$  (dotted) and bayerite (dash-dot) with thermodynamic constants from Table 1 are represented together with the adjusted solubility in the presence of H<sub>2</sub>Proto (long dash) and H<sub>2</sub>Gal (dash-dot-dot).

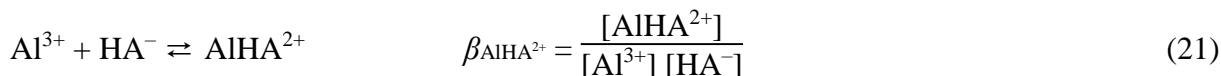
In this work,  $C_{\text{Al,diss}}$  in the supernatant slightly increases as phenolic acid concentration increases similarly for H<sub>2</sub>Phb and H<sub>2</sub>Proto. This evidences that adsorption of phenolic acids slightly favors the mineral dissolution because of Al(III)/acid interaction. In the absence of ligand, dissolution kinetics is controlled by the surface bound protons [9]. Organic acids favor oxide dissolution as they form strong complexes with Al(III) and Fe(III) [9,85], inducing their detachment from the surface. More precisely, organic ligands that bind in a mononuclear (only one atom from the surface is involved), multidentate (two atoms from the ligand are involved), inner-sphere manner significantly increased mineral dissolution [13] by bringing electron density into the coordination sphere of the surface metal. This process weakens the Al-O bond and enhances the release of the metal ion into the bulk solution [11]. By contrast, ligands interacting with the surface atoms in a binuclear, multidentate manner tend to inhibit mineral dissolution as the energy needed to detach simultaneously two Al(III), or Fe(III), atoms from the oxide matrix is higher than the one needed to detach one matrix ion [11,13,85]. Formation of five and six-membered chelate rings (for example with oxalate, catechol, malonate and salicylate) enhanced the dissolution reaction [9]. Some exception can, however, be found; Molis *et al.* [12] showed that adsorption of salicylate onto gibbsite occurs *via* both monodentate and chelate mode and that binuclear complexes are formed, whereas oxide dissolution is favored as salicylate concentration increases in their study.

Bidentate complexes, *via* the carboxylate function, were evidenced for adsorption of H<sub>2</sub>Phb onto goethite [29] and hematite [25], and for adsorption of H<sub>2</sub>Proto onto aluminum hydroxide [33]. Kung and Mc Bride [25] showed that H<sub>2</sub>Phb was adsorbed onto hematite via the

carboxylate group. However, they showed that binuclear complexes were formed as H<sub>2</sub>Phb adsorbs onto hematite, which should not promote dissolution of the oxide. Guan *et al.* [33] showed that bidentate mononuclear complexes were formed between H<sub>2</sub>Proto and Al<sub>2</sub>O<sub>3</sub> surface sites involving the carboxylate group of the acid for low pH. They also showed that, as pH increases, the two phenolate groups of H<sub>2</sub>Proto are involved for adsorption of this acid onto Al<sub>2</sub>O<sub>3</sub>. The same conclusions were drawn by Borah *et al.* [31].

As a rationale, in this work, the increase in the mineral dissolution with acid concentration argues in favor of mononuclear bidentate complexes formation, *i.e.* complexes involving only one Al atom of the surface and two oxygens from the carboxylic function. Moreover, the formation of five membered chelate rings involving Al(III) and two O<sub>phen</sub> could be contemplated for H<sub>2</sub>Proto at high pH. In our modeling, when the carboxylic function is involved a monodentate complex is postulated. The use of models based on Pauling valence rules [71,86] could help in a more physico-chemical realistic description of the adsorption phenomenon. Nevertheless, in the framework of our operational approach, the comprehension of the system is sufficiently sound.

An attempt of fitting experimental concentration of dissolved Al, C<sub>Al,diss</sub>, obtained in the two binary H<sub>2</sub>Proto/Al<sub>2</sub>O<sub>3</sub> and H<sub>2</sub>Phb/Al<sub>2</sub>O<sub>3</sub> systems was carried out, using speciation calculated from Table 1. Pure α-Al<sub>2</sub>O<sub>3</sub> was considered and adsorption of the acids was neglected (1.5 10<sup>-5</sup> mol.L<sup>-1</sup> for H<sub>2</sub>Phb from determined log<sub>10</sub><sup>int</sup>K). The considered reaction for the complex formation was,



where HA<sup>-</sup> is the carboxylate form of H<sub>2</sub>A, which stands for H<sub>2</sub>Phb, H<sub>2</sub>Proto, and H<sub>2</sub>Gal.

[HA<sup>-</sup>] was calculated from,

$$[\text{HA}^{-}] = \frac{[\text{H}_2\text{A}]_{\text{tot}}}{1 + \frac{[\text{H}^{+}]}{K_a}} \quad (22)$$

and the C<sub>Al,diss</sub> were fitted using,

$$C_{\text{Al,diss}} = [\text{Al}^{3+}] (\alpha + \beta_{\text{AlHA}^{2+}} [\text{HA}^{-}]) \quad (23)$$

where

$$\alpha = \left( 1 + \sum_{n \geq 1} \frac{* \beta_n}{[\text{H}^{+}]^n} \right) \quad (24)$$

calculated from the thermodynamic constantes in Table 1. The total concentration of dissolved Al for α-Al<sub>2</sub>O<sub>3</sub> is

$$C_{\text{Al,diss}} = (K_{\text{s},\alpha\text{-Al}_2\text{O}_3})^{1/2} \left( \alpha + \beta_{\text{AlHA}^{2+}} \frac{[\text{H}_2\text{A}]_{\text{tot}}}{1 + \frac{[\text{H}^+]}{K_a}} \right) [\text{H}^+]^3 \quad (25)$$

One can note that the same kind of calculation can be done for bayerite, but the  $\log_{10}\beta_{\text{AlHA}^{2+}}$  values will be higher — about one order of magnitude — as the solubility is lower.

Under these hypotheses, the conditional value of  $\log_{10}\beta_{\text{AlHA}^{2+}}$  is determined by minimizing sum of squares between experimental data and calculation. When accounting for all the data points for H<sub>2</sub>Proto and H<sub>2</sub>Gal – given the low number of H<sub>2</sub>Phb data point it is not reasonable to propose a fit –, the fitting may appear satisfactory but the repartitions of the residuals are clearly biased (not shown). It appears that Al<sup>3+</sup> is dissolved up to a certain value where another phenomenon occurs. One could think about the sorption of the formed complex onto the adsorption sites already determined by titration, but it is unlikely because it is limited to 1.7 sites.nm<sup>-2</sup>, *i.e.* 1.5 10<sup>-5</sup> mol<sub>site</sub>.L<sup>-1</sup>. Nevertheless, more sites are awaited from crystallographic data (*vide ante*) [71], which can participate to such reactions. To determine the  $\log_{10}\beta_{\text{AlHA}^{2+}}$  value, it would seem more reasonable to adjust on the lowest concentration of acid, *i.e.* up to *ca.* 3 mmol/L. The results are presented in Figure 11. In the view of the dispersion of  $C_{\text{Al,diss}}$  with no ligand, the best estimated values of  $\log_{10}\beta_{\text{AlHProto}^{2+}} = 3.6$  and  $\log_{10}\beta_{\text{AlHGal}^{2+}} = 2.8$  was obtained; solubility values for H<sub>2</sub>Phb seem to be in agreement with the evolution in the presence of H<sub>2</sub>Proto. It does not seem reasonable for the time being to back extrapolate these  $\log_{10}\beta$  values to 0 ionic strength as it would require a better determination of the solid phase that controls Al solubility.

Nevertheless, this suggests that the formation of AlHA<sup>2+</sup> complexes is not the only process occurring in the mineral dissolution. For low surface coverage ( $[\text{H}_2\text{A}] < 3 \text{ mmol.L}^{-1}$ ), the presence of acids favors dissolution, but for higher surface coverage the dissolution process is inhibited possibly because AlHA<sup>2+</sup> complex formed in solution can be sorbed onto the surface, but also because the ligand exchange on the surface is very rapid, as ligand concentration is very high and all ionizable surface sites are occupied, and do not permit the detachment of Al atom from the surface. Pyromellitic acid [13] (1,2,4,5-benzenetricarboxylic acid) and maleic acid [67] (Z-butenedioic acid) were shown to inhibit alumina dissolution when they are strongly associated with the alumina surface; these ligands can form multidentate complexes both the surface and with Al<sup>3+</sup>. It is worth noting that contrary to our work, the inhibition of dissolution was observed for all studied concentrations for pyromellitic [13] and maleic [67] acids.

For our system, from an operational point of view, we can model the both the sorption of phenolic acids and the dissolution of the mineral phases by the formation of a complex in solution, even if a clear deviation from the awaited dissolution process is operating. This would require further development as the evidence of the adsorption process at high acid concentration.

## 5 CONCLUSION

The operational characterization of  $\alpha,\gamma\text{-Al}_2\text{O}_3$  particles emphasized a difference in the PZSE (pH 8.5) and IEP (pH 9.5) values that can be caused by the heterogeneity of the oxide

(presence of two crystallographic phases and potentially of impurities). At pH 5, one type of adsorption site for H<sub>2</sub>Phb and H<sub>2</sub>Proto, and two adsorption sites for adsorption of H<sub>2</sub>Gal, were evidenced onto the mineral. The affinity of H<sub>2</sub>Phb toward the surface sites was lower than that of H<sub>2</sub>Proto. Adsorption of H<sub>2</sub>Phb decreased vs. pH, whereas adsorption of H<sub>2</sub>Proto remained approximately constant in pH range 3-7. For the binary systems, three surface complexes were taken into account to describe their properties. The mineral dissolution was favored in the presence of phenolic acids for concentrations lower than *ca.* 3 mmol.L<sup>-1</sup>, but the dissolution is hindered for higher concentrations. These data could be used in view of modeling ternary systems which contain a phenolic acid, a mineral surface, and a metal which can undertake both complexation by the ligand and sorption by the mineral in a further study.

## ACKNOWLEDGEMENTS.

This work was supported by the RSTB program (RBPCCH project) from the CEA, and the French Direction Générale de l'Armement (DGA). Michel Tabarant and Hawa Badji (CEA/DEN/DANS/SEARS/LISL) are acknowledged for their help and assistance during the ICP-AES measurements.

## REFERENCES

- [1] C.R. Jejurkar, I.P. Mavani, P.K. Bhattacharya, Some metal complexes with catechol, pyrogallol, 2,3-dihydroxynaphthalene & protocatechuic acid, *Indian J. Chem.* 10 (1972) 1190-1192.
- [2] Y. Hasegawa, Y. Morita, M. Hase, M. Nagata, Complexation of lanthanoid(III) with substituted benzoic or phenylacetic acids and extraction of these acids, *Bull. Chem. Soc. Jpn.* 62 (1989) 1486-1491.
- [3] Z.M. Wang, L.J. van de Burgt, G.R. Choppin, Spectroscopic study of lanthanide(III) complexes with carboxylic acids, *Inorg. Chim. Acta* 293 (1999) 167-177.
- [4] N. Aoyagi, T. Toraishi, G. Geipel, H. Hotokezaka, S. Nagasaki, S. Tanaka, Fluorescence characteristics of complex formation of europium(III)-salicylate, *Radiochim. Acta* 92 (2004) 589-593.
- [5] R. Aydin, U. Ozer, Potentiometric and spectroscopic studies on yttrium(III) complexes of dihydroxybenzoic acids, *Chem. Pharm. Bull.* 52 (2004) 33-37.
- [6] B. Marmodée, J.S. de Klerk, F. Ariese, C. Gooijer, M.U. Kumke, High-resolution steady-state and time-resolved luminescence studies on the complexes of Eu(III) with aromatic or aliphatic carboxylic acids, *Anal. Chim. Acta* 652 (2009) 285-294.
- [7] S. Kuke, B. Marmodée, S. Eidner, U. Schilde, M.U. Kumke, Intramolecular deactivation processes in complexes of salicylic acid or glycolic acid with Eu(III), *Spectrochim. Acta, Part A* 75 (2010) 1333-1340.
- [8] P.A. Primus, M.U. Kumke, Flash photolysis study of complexes between salicylic acid and lanthanide ions in water, *J. Phys. Chem. A* 116 (2012) 1176-1182.
- [9] G. Furrer, W. Stumm, The coordination chemistry of weathering: I. Dissolution kinetics of  $\delta$ -Al<sub>2</sub>O<sub>3</sub> and BeO, *Geochim. Cosmochim. Acta* 50 (1986) 1847-1860.
- [10] W. Stumm, J.J. Morgan, *Aquatic Chemistry: Chemical Equilibria and Rates in Natural Waters*, Wiley Interscience, New York, NY, USA, 1996.
- [11] W. Stumm, Reactivity at the mineral-water interface: Dissolution and inhibition, *Colloids Surf. A* 120 (1997) 143-166.

- [12] E. Molis, O. Barres, H. Marchand, E. Sauzeat, B. Humbert, F. Thomas, Initial steps of ligand-promoted dissolution of gibbsite, *Colloids Surf. A* 163 (2000) 283-292.
- [13] S.B. Johnson, T.H. Yoon, G.E. Brown, Adsorption of organic matter at mineral/water interfaces: 5. Effects of adsorbed natural organic matter analogues on mineral dissolution, *Langmuir* 21 (2005) 2811-2821.
- [14] I. Kogel, W. Zech, The phenolic acid content of cashew leaves (*Anacardium-Occidentale* L) and of the associated humus layer, Senegal, *Geoderma* 35 (1985) 119-125.
- [15] R. Riffaldi, A. Saviozzi, R. Leviminzi, Retention of coumaric acid by soil and its colloidal components, *Water Air Soil Pollut.* 51 (1990) 307-314.
- [16] B.W. Strobel, Influence of vegetation on low-molecular-weight carboxylic acids in soil solution - a review, *Geoderma* 99 (2001) 169-198.
- [17] K. Suominen, V. Kitunen, A. Smolander, Characteristics of dissolved organic matter and phenolic compounds in forest soils under silver birch (*Betula pendula*), Norway spruce (*Picea abies*) and Scots pine (*Pinus sylvestris*), *Eur. J. Soil Sci.* 54 (2003) 287-293.
- [18] D.R. Bedgood, A.G. Bishop, P.D. Prenzler, K. Robards, Analytical approaches to the determination of simple biophenols in forest trees such as *Acer* (maple), *Betula* (birch), *Coniferus*, *Eucalyptus*, *Juniperus* (cedar), *Picea* (spruce) and *Quercus* (oak), *Analyst* 130 (2005) 809-823.
- [19] R.G. Qualls, Biodegradability of dissolved organic from decomposing fractions of carbon leached leaf litter, *Environ. Sci. Technol.* 39 (2005) 1616-1622.
- [20] F.A. Hassan, A. Ismail, A. Abdulhamid, A. Azlan, Identification and quantification of phenolic compounds in bambangan (*Mangifera pajang* Kort.) peels and their free radical scavenging activity, *J. Agric. Food Chem.* 59 (2011) 9102-9111.
- [21] R. Kummert, W. Stumm, The surface complexation of organic acids on hydrous  $\gamma$ - $\text{Al}_2\text{O}_3$ , *J. Colloid Interface Sci.* 75 (1980) 373-385.
- [22] C.P. Schulthess, J.F. McCarthy, Competitive adsorption of aqueous carbonic and acetic acids by an aluminum oxide, *Soil Sci. Soc. Am. J.* 54 (1990) 688-694.
- [23] B. Gu, J. Schmitt, Z. Chen, L.Y. Liang, J.F. McCarthy, Adsorption and desorption of different organic matter fractions on Iron oxide, *Geochim. Cosmochim. Acta* 59 (1995) 219-229.
- [24] C. Alliot, L. Bion, F. Mercier, P. Toulhoat, Sorption of aqueous carbonic, acetic, and oxalic acids onto  $\alpha$ -alumina, *J. Colloid Interface Sci.* 287 (2005) 444-451.
- [25] K.H. Kung, M.B. McBride, Coordination complexes of *p*-hydroxybenzoate on Fe oxides, *Clays Clay Miner.* 37 (1989) 333-340.
- [26] P.C. Hidber, T.J. Graule, L.J. Gauckler, Influence of the dispersant structure on properties of electrostatically stabilized aqueous alumina suspensions, *J. Eur. Ceram. Soc.* 17 (1997) 239-249.
- [27] C.R. Evanko, D.A. Dzombak, Influence of structural features on sorption of NOM-analogue organic acids to goethite, *Environ. Sci. Technol.* 32 (1998) 2846-2855.
- [28] M.R. Das, O.P. Sahu, P.C. Borthakur, S. Mahiuddin, Kinetics and adsorption behaviour of salicylate on  $\alpha$ -alumina in aqueous medium, *Colloids Surf. A* 237 (2004) 23-31.
- [29] M.R. Das, S. Mahiuddin, The influence of functionality on the adsorption of *p*-hydroxy benzoate and phthalate at the hematite–electrolyte interface, *J. Colloid Interface Sci.* 306 (2007) 205-215.
- [30] M.R. Das, J.M. Borah, W. Kunz, B.W. Ninham, S. Mahiuddin, Ion specificity of the zeta potential of  $\alpha$ -alumina, and of the adsorption of *p*-hydroxybenzoate at the  $\alpha$ -alumina-water interface, *J. Colloid Interface Sci.* 344 (2010) 482-491.
- [31] J.M. Borah, J. Sarma, S. Mahiuddin, Adsorption comparison at the  $\alpha$ -alumina/water interface: 3,4-dihydroxybenzoic acid vs. catechol, *Colloids Surf. A* 387 (2011) 50-56.

- [32] J.M. Borah, J. Sarma, S. Mahiuddin, Influence of functional groups on the adsorption behaviour of substituted benzoic acids at the  $\alpha$ -alumina/water interface, *Colloids Surf. A* 375 (2011) 42-49.
- [33] X.H. Guan, C. Shang, G.H. Chen, ATR-FTIR investigation of the role of phenolic groups in the interaction of some NOM model compounds with aluminum hydroxide, *Chemosphere* 65 (2006) 2074-2081.
- [34] M.V. Biber, W. Stumm, An in-situ ATR-FTIR study: The surface coordination of salicylic acid on aluminum and iron(III) oxides, *Environ. Sci. Technol.* 28 (1994) 763-768.
- [35] T.J. Reich, C.M. Koretsky, Adsorption of Cr(VI) on  $\gamma$ -alumina in the presence and absence of CO<sub>2</sub>: Comparison of three surface complexation models, *Geochim. Cosmochim. Acta* 75 (2011) 7006-7017.
- [36] M. Marques Fernandes, T. Stumpf, B. Baeyens, C. Walther, M.H. Bradbury, Spectroscopic identification of ternary Cm-carbonate surface complexes, *Environ. Sci. Technol.* 44 (2010) 921-927.
- [37] N. Marmier, J. Dumonceau, F. Fromage, Surface complexation modeling of Yb(III) sorption and desorption on hematite and alumina, *J. Contam. Hydrol.* 26 (1997) 159-167.
- [38] T. Rabung, T. Stumpf, H. Geckeis, R. Klenze, J.I. Kim, Sorption of Am(III) and Eu(III) onto  $\gamma$ -alumina: experiment and modelling, *Radiochim. Acta* 88 (2000) 711-716.
- [39] C.W. Davies, *Ion Association*, Butterworths, London, UK, 1962.
- [40] R. Guillaumont, T. Fanghänel, V. Neck, J. Fuger, D.A. Palmer, I. Grenthe, M.H. Rand, *Update on the Chemical Thermodynamics of Uranium, Neptunium, Plutonium, Americium and Technetium*, Elsevier, Amsterdam, 2003.
- [41] Q.Y. Chen, W.M. Zeng, X.M. Chen, S.Q. Gu, G.Q. Yang, H.F. Zhou, Z.L. Yin, Investigation of the thermodynamic properties of  $\gamma$ -Al<sub>2</sub>O<sub>3</sub>, *Thermochim. Acta* 253 (1995) 33-39.
- [42] G. Verdes, R. Gout, S. Castet, Thermodynamic properties of the aluminate ion and of bayerite, boehmite, diaspore and gibbsite, *Eur. J. Miner.* 4 (1992) 767-792.
- [43] S. Castet, J.L. Dandurand, J. Schott, R. Gout, Boehmite solubility and aqueous aluminum speciation in hydrothermal solutions (90-350°C): Experimental study and modeling, *Geochim. Cosmochim. Acta* 57 (1993) 4869-4884.
- [44] G. Lefèvre, M. Duc, P. Lepeut, R. Caplain, M. Fedoroff, Hydration of  $\gamma$ -alumina in water and its effects on surface reactivity, *Langmuir* 18 (2002) 7530-7537.
- [45] F. Adekola, M. Fedoroff, H. Geckeis, T. Kupcik, G. Lefèvre, J. Lützenkirchen, M. Plaschke, T. Preocanin, T. Rabung, D. Schild, Characterization of acid-base properties of two gibbsite samples in the context of literature results, *J. Colloid Interface Sci.* 354 (2011) 306-317.
- [46] G. Lefèvre, M. Duc, M. Fédoroff, Accuracy in the determination of acid-base properties of metal oxides surfaces, In: J. Lützenkirchen (Ed.) *Surface Complexation Modelling*, Elsevier, Amsterdam, The Netherlands, 2006, pp. 35-66.
- [47] X. Carrier, E. Marceau, J.F. Lambert, M. Che, Transformations of  $\gamma$ -alumina in aqueous suspensions: 1. Alumina chemical weathering studied as a function of pH, *J. Colloid Interface Sci.* 308 (2007) 429-437.
- [48] A. Herbelin, J. Westall, FITEQL 4.0: A computer program for determination of chemical equilibrium constant from experimental data, Department of Chemistry, Oregon State University, Corvallis, Oregon, USA, 1994.
- [49] G. Sposito, *The Environmental Chemistry of Aluminium*, Lewis Publishers, Boca Raton, FL, USA, 1996.
- [50] J. Lützenkirchen, The constant capacitance model and variable ionic strength: An evaluation of possible applications and applicability, *J. Colloid Interface Sci.* 217 (1999) 8-18.
- [51] W. Stumm, C.P. Huang, S.R. Jenkins, Specific chemical interactions affecting the stability of dispersed systems, *Croat. Chem. Acta* 42 (1970) 223-244.
- [52] C.P. Huang, W. Stumm, Specific adsorption of cations on hydrous  $\gamma$ -Al<sub>2</sub>O<sub>3</sub>, *J. Colloid Interface Sci.* 43 (1973) 409-420.

- [53] R.J. Hunter, *Zeta Potential in Colloid Science. Principles and Applications*, Academic Press, London, UK, 1981.
- [54] F. Booth, The dielectric constant of water and the saturation effect, *J. Chem. Phys.* 19 (1951) 391-394.
- [55] M. Flörsheimer, K. Kruse, R. Polly, A. Abdelmonem, B. Schimmelpfennig, R. Klenze, T. Fanghänel, Hydration of mineral surfaces probed at the molecular level, *Langmuir* 24 (2008) 13434-13439.
- [56] A. Breeuwsma, J. Lyklema, Physical and chemical adsorption of ions in electrical double-layer on hematite ( $\alpha$ -Fe<sub>2</sub>O<sub>3</sub>), *J. Colloid Interface Sci.* 43 (1973) 437-448.
- [57] A. Naveau, F. Monteil-Rivera, J. Dumonceau, S. Boudesocque, Sorption of europium on a goethite surface: influence of background electrolyte, *J. Contam. Hydrol.* 77 (2005) 1-16.
- [58] J. Jiang, R.K. Xu, S.Z. Li, Effect of ionic strength and mechanism of Cu(II) adsorption by goethite and  $\gamma$ -Al<sub>2</sub>O<sub>3</sub>, *J. Chem. Eng. Data* 55 (2010) 5547-5552.
- [59] J.F. Boily, J.B. Fein, Adsorption of Pb(II) and benzenecarboxylates onto corundum, *Chem. Geol.* 148 (1998) 157-175.
- [60] X. Wang, W. Dong, X. Dai, A. Wang, J. Du, Z. Tao, Sorption and desorption of Eu and Yb on alumina: mechanisms and effect of fulvic acid, *Appl. Radiat. Isot.* 52 (2000) 165-173.
- [61] D. Xu, Q.L. Ning, X. Zhou, C.L. Chen, X.L. Tan, A.D. Wu, X. Wang, Sorption and desorption of Eu(III) on alumina, *J. Radioanal. Nucl. Chem.* 266 (2005) 419-424.
- [62] C. Alliot, L. Bion, F. Mercier, P. Toulhoat, Effect of aqueous acetic, oxalic, and carbonic acids on the adsorption of europium(III) onto  $\alpha$ -alumina, *J. Colloid Interface Sci.* 298 (2006) 573-581.
- [63] N. Janot, P.E. Reiller, M.F. Benedetti, Modeling Eu(III) speciation in a Eu(III)/humic acid/ $\alpha$ -Al<sub>2</sub>O<sub>3</sub> ternary system, *Colloids Surf. A*, this issue (2013).
- [64] M. Kosmulski, Compilation of PZC and IEP of sparingly soluble metal oxides and hydroxides from literature, *Adv. Colloid Interface Sci.* 152 (2009) 14-25.
- [65] M. Kosmulski, The pH-dependent surface charging and points of zero charge: V. Update, *J. Colloid Interface Sci.* 353 (2011) 1-15.
- [66] E. Tombácz, M. Szekeres, Interfacial acid-base reactions of aluminum oxide dispersed in aqueous electrolyte solutions. 1. Potentiometric study on the effect of impurity and dissolution of solid phase, *Langmuir* 17 (2001) 1411-1419.
- [67] S.B. Johnson, T.H. Yoon, B.D. Kocar, G.E. Brown, Adsorption of organic matter at mineral/water interfaces. 2. Outer-sphere adsorption of maleate and implications for dissolution processes, *Langmuir* 20 (2004) 4996-5006.
- [68] A.A. Jara, S. Goldberg, M.L. Mora, Studies of the surface charge of amorphous aluminosilicates using surface complexation models, *J. Colloid Interface Sci.* 292 (2005) 160-170.
- [69] X.F. Yang, Z.X. Sun, D.S. Wang, W. Forsling, Surface acid-base properties and hydration/dehydration mechanisms of aluminum (hydr)oxides, *J. Colloid Interface Sci.* 308 (2007) 395-404.
- [70] R. Wood, D. Fornasiero, J. Ralston, Electrochemistry of the boehmite-water interface, *Colloids Surf.* 51 (1990) 389-403.
- [71] T. Hiemstra, H. Yong, W.H. van Riemsdijk, Interfacial charging phenomena of aluminum (hydr)oxides, *Langmuir* 15 (1999) 5942-5955.
- [72] L. Borgnino, C.P. De Pauli, P.J. Depetris, Arsenate adsorption at the sediment-water interface: sorption experiments and modelling, *Environ. Earth Sci.* 65 (2012) 441-451.
- [73] E. Hückel, Die Kataphorese des Kugel, *Z. Phys.* 25 (1924) 204-210.
- [74] H. Ohshima, A simple expression for Henry's function for the retardation effect in electrophoresis of spherical colloidal particles, *J. Colloid Interface Sci.* 168 (1994) 269-271.

- [75] G.A. Parks, Isoelectric points of solid oxides solid hydroxides and aqueous hydroxo complex systems, *Chem. Rev.* 65 (1965) 177-198.
- [76] J.A. Davis, R.O. James, J.O. Leckie, Surface ionization and complexation at the oxide/water interface. I. Computation of electrical double layer properties in simple electrolytes, *J. Colloid Interface Sci.* 63 (1978) 480-499.
- [77] G.A. Parks, Surface energy and adsorption at mineral/water interfaces: An introduction, In: M.F. Hochella, Jr., A.F. White (Eds.) *Mineral-Water Interface Geochemistry*, Mineralogical Society of America, Washington, DC, USA, 1990.
- [78] W. Stumm, R. Kummert, L. Sigg, A ligand-exchange model for the adsorption of inorganic and organic ligands at hydrous oxide interfaces, *Croat. Chem. Acta* 53 (1980) 291-312.
- [79] T.H. Yoon, S.B. Johnson, C.B. Musgrave, G.E. Brown, Jr., Adsorption of organic matter at mineral/water interfaces: I. ATR-FTIR spectroscopic and quantum chemical study of oxalate adsorbed at boehmite/water and corundum/water interfaces, *Geochim. Cosmochim. Acta* 68 (2004) 4505-4518.
- [80] J.A. Davis, J.O. Leckie, Effect of adsorbed complexing ligands on trace metal uptake by hydrous oxides, *Environ. Sci. Technol.* 12 (1978) 1309-1315.
- [81] M.S. Lucas, A.A. Dias, R.M. Bezerra, J.A. Peres, Gallic acid photochemical oxidation as a model compound of winery wastewaters, *J. Environ. Sci. Health, Part A* 43 (2008) 1288-1295.
- [82] V. Tulyathan, R.B. Boulton, V.L. Singleton, Oxygen-uptake by gallic acid as a model for similar reactions in wines, *J. Agric. Food Chem.* 37 (1989) 844-849.
- [83] P. Moreau, Etude des interactions entre Eu(III) et des particules d'Al<sub>2</sub>O<sub>3</sub> en présence d'acides phénoliques, PhD Thesis, Chimie Physique et Chimie Analytique, Université Pierre et Marie Curie (Paris VI), Paris, France, 2012, pp. 263, <http://tel.archives-ouvertes.fr/tel-00789479>.
- [84] F.J. Benitez, J. Beltran-Heredia, J.L. Acero, T. Gonzalez, Degradation of protocatechuic acid by two advanced oxidation processes: Ozone/UV radiation and H<sub>2</sub>O<sub>2</sub>/UV radiation, *Water Res.* 30 (1996) 1597-1604.
- [85] W. Stumm, The inner sphere surface complex - A key to understanding surface reactivity, In: C.P. Huang, C.R. O'Melia, J.J. Morgan (Eds.) *Aquatic Chemistry - Interfacial and Interspecies Processes*, American Chemical Society, Washington, DC, USA, 1995, pp. 1-32.
- [86] S.B. Johnson, T.H. Yoon, A.J. Slowey, G.E. Brown, Adsorption of organic matter at mineral/water interfaces: 3. Implications of surface dissolution for adsorption of oxalate, *Langmuir* 20 (2004) 11480-11492.